Field Oriented Control of Induction Motors Based on DSP Controller

by Vamsi Krishna Pavuluri, Bachelor of Science

A Thesis Submitted in Partial
Fulfillment of the Requirements
for the Degree of
Master of Science
in the field of Electrical Engineering

Advisory Committee:

Xin Wang, Chair

George L. Engel

Robert Leander

Graduate School
Southern Illinois University Edwardsville

December, 2014

ABSTRACT

FIELD ORIENTED CONTROL OF INDUCTION MOTORS BASED ON DSP CONTROLLER

by

VAMSI KRISHNA PAVULURI

Chairperson: Professor Xin Wang

Induction Motor is the most widely used industrial workhorse due to its reliability and high robustness, low cost and good efficiency. Field oriented control technique (FOC) of AC machines facilitates the dynamic control of induction motor. Field oriented control improves the dynamic performance of an induction motor and is commonly used method for speed and torque control applications.

In this thesis, the basic concepts and equivalent circuit model of squirrel cage induction motor are explained. A mathematical model is developed for squirrel cage induction motor. The Clarke's and Park's transformations are used to convert *abc* reference frame into *dq* rotating coordinate frame. The three-phase inverter, which supplies desired voltage/current to the stator winding is designed based on Pulse Width Modulation (PWM). The space vector PWM technique is implemented for controlling the three-phase inverter switches, which is simulated using Matlab/Simulink.

Field oriented control method is developed to get the decoupled control of flux and torque, which is comparable to the DC motor. The direct and indirect field oriented control methods are presented to obtain rotor flux angle. In this thesis, a novel field oriented control scheme for induction motor is developed. PID based controllers are designed for speed and current control loop based on symmetrical optimum method, which guarantee the maximum phase margin. The control approach can be applied to both direct and indirect field oriented control of induction machines. The computer simulations are used to show the efficacy of the proposed algorithm.

The developed field oriented control method is implemented using Texas Instrument AC motor development kit and software. A short review is presented on high voltage motor control board and DSP controllers. The field oriented control of induction motor shows satisfactory performance based on computer simulation and hardware implementation results.

ACKNOWLEDGEMENTS

I would like to sincerely appreciate my thesis advisor Dr. Xin Wang for his continuous support, motivation and guidance during my research. With his assistance and involvement helped me to accomplish this thesis.

I would also like to thank my thesis committee: Dr. George L. Engel and Dr. Robert Leander for their help. In addition, I would like thank my research classmates and my special friends.

Most importantly, I would like to express my deepest thanks to my parents and friends for their support. Finally, I would like to dedicate this work to my grand parents.

TABLE OF CONTENTS

LIST OF FIGURES

LIST OF TABLES

CHAPTER 1

INTRODUCTION

Induction machines have been widely used as industrial workhorse, at least 90% of industrial drive systems employ induction motors due to low cost and high robustness compared with other electric machines. Typically, induction motors have an exceptional torque reserve and load dependence of speed. The induction motor consists of stator

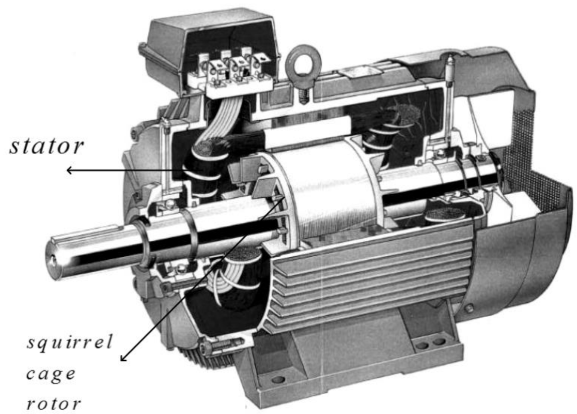

Figure 1.1: The Cut View of Squirrel Cage Induction Motor

and rotor winding. The stator produces a rotating magnetic field and induces voltage in the rotor similar to a transformer, which makes the rotor turn at a speed less than the synchronous speed. Based on the construction type of the rotor, the induction motors are classified into wound type and squirrel cage type induction motors. In this thesis, the squirrel cage induction motors are considered. The cut view of a squirrel cage induction motor is shown in Fig 1.1.

The speed of induction motor can be controlled by different methods. (V/f) control is most commonly used scalar control method for speed control in which both voltage and flux are varied to keep the ratio constant. The scalar control gives the slower response, more overshoot and suffers instability for higher order harmonics[18]. However, field oriented control or vector control has better performance than scalar control methods. The speed control of induction motor must be done through Adjustable Speed Drives (ASD). The growth and availability of power electronic devices made speed control affordable. This thesis considers the adjustable speed drives based on Space Vector PWM three-phase voltage source inverter as the induction motor drive.

Compared with traditional scalar control (V/f) control approach, the Field Oriented Control (FOC) needs more calculation effort, but has the following advantages:

- full torque control capability at low speed
- better dynamic behavior
- higher efficiency
- operating point in a wide range of speed
- decoupled torque and flux control
- four quadrant operation

The FOC concept, which was first introduced by Hasse in 1969 and Blaschke in 1972, constitutes the most important paradigm in controlling induction motors. Basically, the objective of field orientation is to make induction machine work similar to separately excited DC machines. The reason for implementing this technique on induction motor is to get decoupled control of torque and flux as in separately excited DC motors. The field-oriented control consists of direct and indirect vector control methods. For direct method, the rotor flux angle can be obtained from direct measurement of rotor flux. In this case, the rotor flux angle can be calculated. Alternatively, indirect method obtains the rotor flux angle by exploiting the currents and voltages. Our proposed control approach can be applied to both direct and indirect method.

Many different control techniques based on PID tuning have been developed and used in industrial application during the past decade. The most popular Ziegler-Nicholas method is frequently used in applications. In this case, the model can be characterized as first order transfer function when a step input is applied. This standardized method is easy to implement but may cause significant overshoot or even instability of the system. Many other methods such as fuzzy controller, root locus and pole assignment design techniques, neural network control, e.t.c, have also been developed. The efficacy and performance of these methods limits their applications.

In this thesis, a novel symmetrical optimum method control for induction machines is proposed, which guarantee the maximum phase margin. The first paper on symmetrical optimum method was written by Kessler in 1958 [20] for designing PI and PID controllers as one degree of freedom controllers for benchmark process models. The particular feature of symmetrical optimum method guarantees the closed loop system maximum phase margin and is well suited for electric machine control applications.

1.1 Conclusion

In this thesis, the rotor field oriented control of an induction motor dynamics is developed. By designing the decoupled structure using feed-forward control method, the coefficients of PI controller are designed based on symmetrical optimum methods. Computer simulations are used to show the robustness and effectiveness of our proposed approach. The field oriented control for designed PI controllers is implemented using Texas Instrument AC motor development kit with digital signal processor.

CHAPTER 2

LITERATURE REVIEW

Field oriented control of induction motor is studied in this paper. The basic concepts and equivalent circuit model of induction motor are summarized in [2] [9]. The concept of rotating magnetic field is explained in [9]. The flux linkage and inductance of induction motor are determined in[1] [2] and [11]. The Park's and Clarke's transformation convert *abc* coordinate frame to *dq* coordinate frame are documented in [1] [8]. The dynamic modeling of induction motor can be found in [1] and [3]. The Space Vector PWM switching technique for three phase voltage source inverter are given in [6] [7]. Field oriented control technique of induction motor is introduced in [1] and [29]. The sensored field oriented control of induction motor can be found in [1] [12]. Some preliminary results on the PID controllers designed using symmetrical optimum method have been studied in [20] [21].

The concept of slip and torque speed characteristics is explained in [2][9]. In [1] [2], the mathematical model and dynamic modeling of induction machine using Clarke's and Park's transformations are discussed. The basic concepts of power electronic devices are illustrated in [5][14] and [15]. Different types of inverters and their advantages are discussed in [5] and [16]. The inverter switching techniques such as pulse width modulation(PWM), sinusoidal PWM and space vector PWM are explained in [6] and [7]. The scalar control methods for speed control of induction motor are studied in [1] [2]. The advantages of vector control method over the scalar methods have been studied in [18].

The concept and modeling the field oriented control of induction motor is based on [1]. The comparison of vector control of induction motor to a DC motor is summarized [2]. Some preliminary studies on the decoupled control of induction motor is proposed in [1]. The implementation of field oriented control is based on the sensored field oriented control of induction motor from Texas Instruments report [12]. [20] and [21] discuss the design of PID controllers using symmetrical optimum method. Some earlier research on the speed control of induction motor can be found in [23]-[30]. The Texas Instruments AC motor development kits and software are used to develop the program, and produce control signal in real time [31].

CHAPTER 3

THE MODELING OF INDUCTION MOTOR

3.1 Introduction

An induction motor consists of two parts: stator and rotor winding. The construction of induction motor is different from synchronous motor, since there is no supply to the rotor. Based on construction of the rotor, the induction motor can be classified into two types: one is wound type and the other is cage type. In this thesis, the squirrel cage type induction motors are discussed, since they are the most commonly used electric motors in industry and household. Induction machines do not have permanent magnets, brushes or commutators. They have a wide variety of applications such as blowers, conveyor, cranes, refrigerators, traction and many other industrial applications, because of their high robustness and reliability.

3.1.1 Rotating Magnetic Field

"The rotating magnetic field is produced when at least two phase windings are displaced in space, with currents in these windings displaced in phase" [2]. The stator consists of a three-phase winding placed 120^0 electrically apart. The windings of stator are supplied with a balanced set of three phase currents having equal magnitude and phase difference of 120^0, which are shown in (3.1), (3.2) and (3.3). Stator creates a rotating field B_s with constant magnitude. The windings are distributed sinusoidally to reduce higher order harmonics in magnetomotive force. The arrangement of the stator windings consisting of concentrated winding is shown in Fig. 3.1

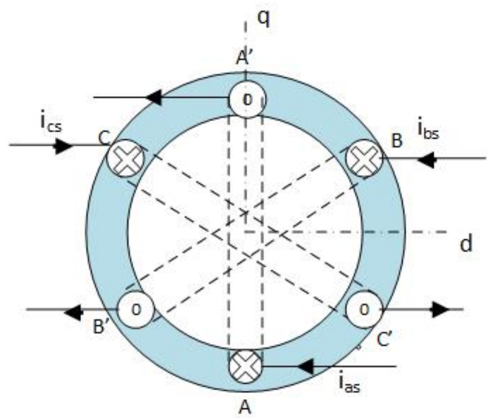

Figure 3.1: The Simple Construction of Two Pole Stator

$$i_{aa'} = I_m sin(\omega t) \tag{3.1}$$

$$i_{bb'} = I_m sin(\omega t - \frac{2\pi}{3}) \tag{3.2}$$

$$i_{cc'} = I_m sin(\omega t - \frac{4\pi}{3}) \tag{3.3}$$

where ω is the angular speed, t is the time, and I_m is current magnitude.

The closed-loop coils carrying AC current produce magnetic field intensity based on Ampere's law. The magnetic field intensities of three currents coils are :

$$H_{aa'} = H_m sin(\omega t) \tag{3.4}$$

$$H_{bb'} = H_m sin(\omega t - \frac{2\pi}{3}) \tag{3.5}$$

$$H_{cc'} = H_m sin(\omega t - \frac{4\pi}{3}) \tag{3.6}$$

From magnetic flux intensity, one can obtain magnetic flux densities based on $B = \mu H$

$$B_{aa'} = B_m sin(\omega t) \tag{3.7}$$

$$B_{bb'} = B_m sin(\omega t - \frac{2\pi}{3}) \tag{3.8}$$

$$B_{cc'} = B_m sin(\omega t - \frac{4\pi}{3}) \tag{3.9}$$

At time ωt=0^0, they have a phase shift of 120^0 from each other. The net magnetic filed density can be obtained by summing up of all three coils magnetic field density vectors.

$$
\begin{aligned}
B_{net} &= B_{aa'} + B_{bb'} + B_{cc'} \\
&= 0 + (\frac{-\sqrt{3}}{2}B_m)\angle 120^0 + \frac{\sqrt{3}}{2}B_m\angle 240^0 \\
&= \frac{\sqrt{3}}{2}B_m[-(cos\frac{\pi}{3})\,\widehat{x} + sin(\frac{\pi}{3})\,\widehat{y} + cos(\frac{2\pi}{3})\,\widehat{x} + sin\frac{2\pi}{3})\,\widehat{y}] \\
&= -\frac{3}{2}\,B_m\,\widehat{y} \\
&= 1.5B_m\angle - 90^0
\end{aligned}
$$

By summing up of all the vectors at time t=0, the resultant vector magnitude is 1.5 B_m at $\angle - 90^0$, which is shown in Fig 3.2. At time $\omega t = 90^0$, the net magnetic field $B_{net} = 1.5B_m\angle 0^0$, which is shown in Fig 3.3. The magnitude of B_{net} remained constant, but the direction of magnetic field density has changed and will continue to rotate with an angular velocity of ω. The magnetic filed rotates at a speed of $n_s = \frac{120f_e}{P}$, where n_s is synchronous speed, f_e is the supply frequency, and P is the number of pole. Thus, the

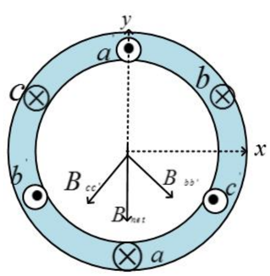

Figure 3.2: At $\omega t = 0$

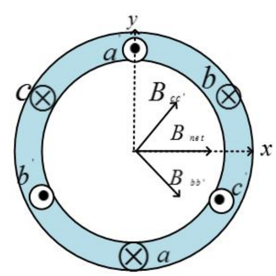

Figure 3.3: At $\omega t = 90^0$

stator produces a rotating magnetic filed.

The relative motion of rotating stator magnetic field with respect to the rotor induces voltage in the rotor conductors according to Faraday's law. The induced EMF produces induced current in the rotors and the magnetic field in the rotor seeks to oppose the change of external magnetic flux, according to Lenz's law. The rotor will start to rotate and tries to catch up with the stator magnetic field.

$$e_{ind} = (v \times B) \cdot l \tag{3.10}$$

v velocity of rotor bars relative to the magnetic field

B magnetic flux density

l length of the conductor

The induced voltage produces current i in the rotor conductors, which induces a force when placed in the external stator magnetic field $F = i(l \times B)$. Based on the right hand rule, the direction of the force acting on the conductor is same as the motion of the rotor magnetic field. The induced EMF is proportional to the change of flux linking to the rotor conductors. If the rotor rotates at synchronous speed, then the relative motion of the rotor to the stator is stationary and the voltage induced is zero. If the induced voltage is zero, then there is no induced current. The operation of induction motor mainly depends upon the relative motion between the stator magnetic field and rotor. The synchronous speed n_s of the motor is denoted as the stator magnetic field speed, n_r is denoted as the rotor speed. The induction machine works as a motor when the rotor moves slower than the synchronous speed. The difference in rpm is defined as slip speed, i.e,

$$n_{slip} = n_s - n_r \tag{3.11}$$

When slip speed is expressed in per unit or percentage value, slip defined by

$$s = \frac{n_s - n_r}{n_s} \times 100\% \tag{3.12}$$

It may also be expressed in angular velocity ω

$$s = \frac{\omega_{syn} - \omega_m}{\omega_{syn}} \times 100\% \tag{3.13}$$

3.1.2 The Equivalent Circuit of Induction Motor

The working principle of a induction motor is similar to a transformer. It is also called a rotating transformer. The stator winding is considered as primary winding and rotor as secondary winding which is always shortened. The voltage induced from primary winding to the secondary winding is just as the voltage induced in transformers. There are a few characteristics such as frequency and air gap, which differentiate induction machine from the real transformers. The air gap exists between the stator and rotor for induction motors. The frequency induced in the rotor varies in induction machine when the rotor is loaded. However, in the transformer, no air gap is presented between the primary and secondary winding, and the electrical frequency is same on both sides. The per-phase equivalent circuit of induction machine is represented in Fig. 3.5.

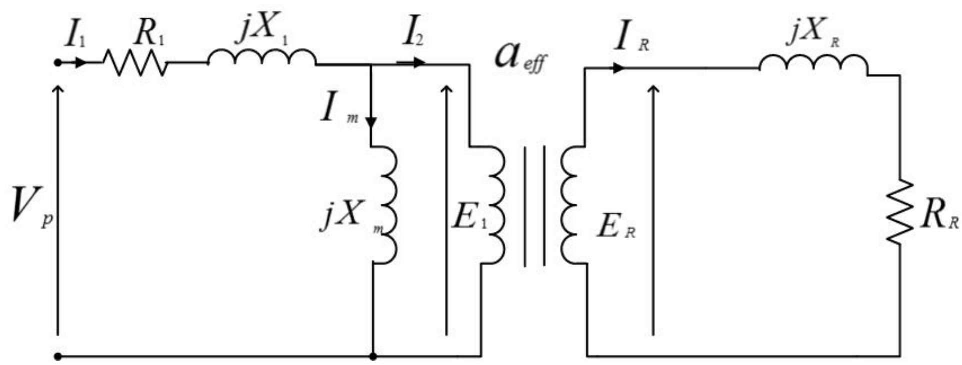

Figure 3.4: The Per Phase Equivalent Circuit of Induction Motor

where

R_1, R_R	stator and rotor resistance
X_1, X_R	stator and rotor leakage reactance
X_m	magnetizing reactance
V_p	voltage supplied to stator
E_1, E_R	stator and rotor EMF
I_1, I_R	stator and rotor currents.

The induced rotor voltage and frequency in rotor winding depends upon the relative motion characterized by the slip s. The slip s is always between 0 and 1 ($0 \leq s \leq 1$) for induction machine to operate in motoring mode. If the rotor is locked, then the largest relative motion occurs and maximum voltage is induced, when slip is equal to 1. Slip is equal to zero when the rotor runs at synchronous speed. The rotor runs at different speeds if applied load is changed, and its induced voltage and frequency is proportional to the slip.

$$E_R = sE_{LR}$$

The resistance of the rotor is independent of slip, but the reactance changes due to the change in rotor frequency.

$$X_R = sX_{LR}$$

The new equivalent circuit is shown in Fig 3.5.

From the secondary side the rotor winding current can be calculated as follows

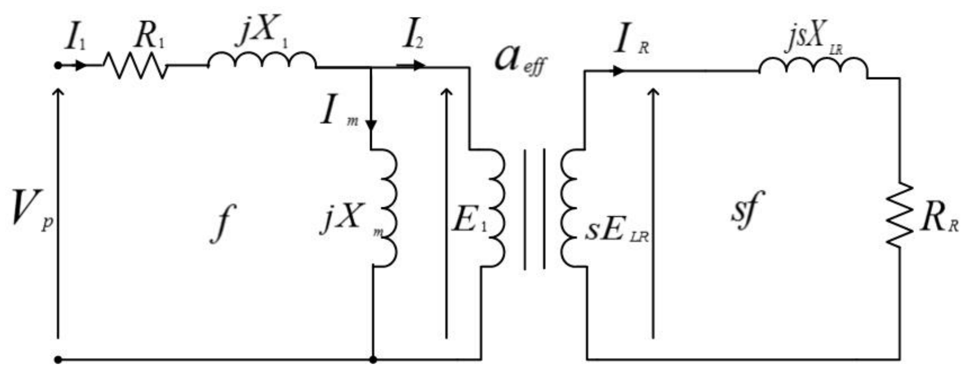

Figure 3.5: The Per Phase Equivalent Circuit of Induction Motor

$$I_R = \frac{sE_{LR}}{R_R + jsX_{LR}} \tag{3.14}$$

Equivalently, we have

$$I_R = \frac{E_{LR}}{\frac{R_R}{s} + sX_{LR}} \tag{3.15}$$

Considering the equivalent turns ratio a_{eff}, the per-phase equivalent circuit of induction motor referring rotor to the stator side is shown in Fig 3.6.

$$R_2 = a_{eff}^2 R_R, X_2 = a_{eff}^2 X_{LR}, I_2 = \frac{1}{a_{eff}} I_R$$

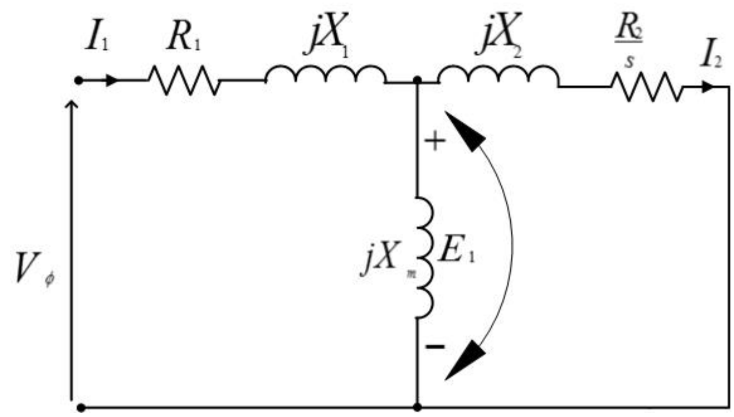

Figure 3.6: The Modified Per Phase Equivalent Circuit of Induction Motor

3.2 Torque-Speed Characteristics

The torque of a machines is generated by electrical to mechanical power conversion. The induced torque is defined as

$$T_{ind} = \frac{P_{gross\_mech}}{\omega_m}$$

where P_{gross_mech} is the gross mechanical power. ω_m is the rotor speed. P_{ag} is power crossing the air gap from stator to the rotor circuit, which is converted to mechanical power and rotor copper losses. The air gap power is calculated from

$$P_{ag} = \frac{3I_2^2 R_2}{s}$$

The mechanical power developed is the gross mechanical power P_{gross_mech}, which can be obtained by subtracting rotor copper losses from P_{ag}.

$$\begin{aligned} P_{gross\_mech} &= \frac{3I_2^2 R_2}{s} - 3I_2^2 R_2 \\ &= \frac{3I_2^2 (1-s) R_2}{s} \end{aligned}$$

The current I_2 can obtained by applying Thevenin's circuit analysis to the equivalent circuit shown in Fig. 3.6

$$|I_2| = \frac{V_{TH}}{\sqrt{(R_{TH} + \frac{R_2}{s})^2 + (X_{TH} + X_2)^2}}$$

The air gap P_{ag} can be calculated by substituting I_2 is

$$P_{ag} = \frac{3V_{TH}^2 \frac{R_2}{s}}{(R_{TH} + \frac{R_2}{s})^2 + (X_{TH} + X_2)^2}$$

The induced torque in rotor is

$$T_{ind} = \frac{P_{ag}}{\omega_s} = \frac{3V_{TH}^2 \frac{R_2}{s}}{\omega_s[(R_{TH} + \frac{R_2}{s})^2 + (X_{TH} + X_2)^2]} \tag{3.16}$$

where V_{TH}, R_{TH} and X_{TH} are Thevenin's voltage, resistance and reactance

$$\begin{aligned} V_{TH} =& V_\phi \frac{X_m}{R_1 + jX_1 + jX_m} \\ R_{TH} =& \frac{R_1 X_m^2}{R_1^2 + (X_1 + X_m)^2} \\ X_{TH} =& X_m \frac{(R_1^2 + X_1(X_1 + X_m))}{R_1^2 + (X_1 + X_m)^2} \end{aligned}$$

3.3 The System Equations in abc Reference Frame

The stator consists of a three-phase winding classified as the a_s, b_s, c_s have the same number of per phase effective turns N_s. Similarly, the rotor consists of three-phase windings a_r, b_r, c_r having the same number of turns per phase N_r, where s and r represents the stator and rotor winding respectively. The voltage equations of the stator and rotor can be written using Kirchoff voltage law, where all three phases are represented in the matrix form as follows

$$v_{abc}^s = r_s i_{abc}^s + \frac{d}{dt} \lambda_{abc}^s \tag{3.17}$$

$$v_{abc}^r = r_r i_{abc}^r + \frac{d}{dt} \lambda_{abc}^r \tag{3.18}$$

where

$$v_{abc}^s = \begin{bmatrix} v_a^s \\ v_b^s \\ v_c^s \end{bmatrix},\ v_{abc}^r = \begin{bmatrix} v_a^r \\ v_b^r \\ v_c^r \end{bmatrix},\ i_{abc}^s = \begin{bmatrix} i_a^s \\ i_b^s \\ i_c^s \end{bmatrix},\ i_{abc}^r = \begin{bmatrix} i_a^r \\ i_b^r \\ i_c^r \end{bmatrix},\ \lambda_{abc}^s = \begin{bmatrix} \lambda_a^s \\ \lambda_b^s \\ \lambda_c^s \end{bmatrix},\ \lambda_{abc}^r = \begin{bmatrix} \lambda_a^r \\ \lambda_b^r \\ \lambda_c^r \end{bmatrix},$$

The terminal voltage is equal to the summation of voltage drop across the winding resistance and back EMF. The flux linkage equation is given as:

$$\lambda = Li \tag{3.19}$$

The time-varying magnetic flux is affected by both of the stator and rotor currents. The coupling between the stator and rotor three phase winding leads to the flux linkage equations as:

$$\lambda_{abc}^s = \lambda_{abc}^s(s) + \lambda_{abc}^s(r) \tag{3.20}$$

$$\lambda_{abc}^r = \lambda_{abc}^r(r) + \lambda_{abc}^r(s) \tag{3.21}$$

where $\lambda_{abc}^s(s)$ is the total flux linkage of stator due to stator current and $\lambda_{abc}^s(r)$ is the total flux linkage of stator due to the rotor current. Similarly, the total flux linkage of rotor is equal to the summation of the flux linkage due to the rotor current $\lambda_{abc}^r(r)$ and the flux linkage due to the stator current $\lambda_{abc}^r(s)$. The corresponding individual flux linkages are shown in the matrix form as follows.

$$\lambda_{abc}^s(s) = \begin{bmatrix} L_{as} & L_{abs} & L_{acs} \\ L_{abs} & L_{bs} & L_{bcs} \\ L_{acs} & L_{bcs} & L_{cs} \end{bmatrix} \begin{bmatrix} i_a^s \\ i_b^s \\ i_c^s \end{bmatrix};\ \lambda_{abc}^s(r) = \begin{bmatrix} L_{as,ar} & L_{as,br} & L_{as,cr} \\ L_{bs,ar} & L_{bs,br} & L_{bs,cr} \\ L_{cs,ar} & L_{cs,br} & L_{cs,cr} \end{bmatrix} \begin{bmatrix} i_a^r \\ i_b^r \\ i_c^r \end{bmatrix};$$

$$\lambda_{abc}^r(r) = \begin{bmatrix} L_{ar} & L_{abr} & L_{acr} \\ L_{abr} & L_{br} & L_{bcr} \\ L_{acr} & L_{bcr} & L_{cr} \end{bmatrix} \begin{bmatrix} i_a^s \\ i_b^s \\ i_c^s \end{bmatrix};\ \lambda_{abc}^r(s) = \begin{bmatrix} L_{ar,as} & L_{ar,bs} & L_{ar,cs} \\ L_{br,as} & L_{br,bs} & L_{br,cs} \\ L_{cr,as} & L_{cr,bs} & L_{cr,cs} \end{bmatrix} \begin{bmatrix} i_a^s \\ i_b^s \\ i_c^s \end{bmatrix}$$

3.4 Determination of Machine Inductances

Each winding has self-inductance and mutual inductance. The inductance due to change of current in its own winding is called self-inductance, and the inductance corresponding to the change of current in the other winding is called the mutual inductance. Now, let's calculate the total inductance of each winding in stator and rotor.

The total self-inductance of a coil is the summation of the leakage and magnetizing inductance. Considering the total self-inductance of stator phase a_s, we can express the total self inductance of phase a_s as

$$L_{as} = L_{ls} + L_{am}$$

Similarly, for phase b_s and c_s of stator

$$L_{bs} = L_{ls} + L_{am}$$

$$L_{cs} = L_{ls} + L_{am}$$

where L_{ls} is the self inductance and L_{ms} is the magnetizing inductance of stator.
The magnetizing inductance of all the phases of the stator are equal in magnitude and can be calculated as

$$L_{am} = L_{bm} = L_{cm} = L_{ms} = \mu_0 N_s^2 \frac{rl}{g}\frac{\pi}{4} \tag{3.22}$$

The mutual inductance between stator three phase windings a_s, b_s and c_s can be calculated as

$$L_{abs} = L_{bcs} = L_{cas} = -\mu_0 N_s^2 \frac{rl}{g}\frac{\pi}{8} = -\frac{L_{ms}}{2} \tag{3.23}$$

The flux linkage of stator winding due to the currents flowing in stator can be written as

$$\lambda^s_{abc}(s) = \begin{bmatrix} L_{ls} + L_{ms} & -\frac{L_{ms}}{2} & -\frac{L_{ms}}{2} \\ -\frac{L_{ms}}{2} & L_{ls} + L_{ms} & -\frac{L_{ms}}{2} \\ -\frac{L_{ms}}{2} & -\frac{L_{ms}}{2} & L_{ls} + L_{ms} \end{bmatrix} \begin{bmatrix} i^s_a \\ i^s_b \\ i^s_c \end{bmatrix} \tag{3.24}$$

Now, Let's calculate the mutual inductance between rotor and stator windings. Consider that the rotor phase a_r is displaced by an angle θ_r from the stator phase a_s winding. Similarly, b_r and c_r are displaced from b_s and c_s by θ_r.

The corresponding mutual inductances can be calculated as

$$L_{as,ar} = L_{bs,br} = L_{cs,cr} = \mu_0 N_s N_r \frac{rl}{g}\frac{\pi}{4} cos\theta_r = \frac{N_r}{N_s} L_{ms} cos\theta_r$$

The angle between the phase a_s and b_r phase is $(\theta_r + \frac{2\pi}{3})$. Similarly, the angle between the a_s and c_r phase is $(\theta_r - \frac{2\pi}{3})$.

$$L_{as,br} = L_{bs,cr} = L_{cs,ar} = \frac{N_r}{N_s} L_{ms} cos(\theta_r + \frac{2\pi}{3})$$
$$L_{as,cr} = L_{bs,ar} = L_{cs,br} = \frac{N_r}{N_s} L_{ms} cos(\theta_r - \frac{2\pi}{3})$$

The calculated flux linkages of the stator phases due to the rotor currents can be written in the matrix form as

$$\lambda^s_{abc}(r) = \frac{N_r}{N_s} L_{ms} \begin{bmatrix} cos\theta_r & cos(\theta_r + \frac{2\pi}{3}) & cos(\theta_r - \frac{2\pi}{3}) \\ cos(\theta_r - \frac{2\pi}{3}) & cos\theta_r & cos(\theta_r + \frac{2\pi}{3}) \\ cos(\theta_r + \frac{2\pi}{3}) & cos(\theta_r - \frac{2\pi}{3}) & cos\theta_r \end{bmatrix} \begin{bmatrix} i^r_a \\ i^r_b \\ i^r_c \end{bmatrix} \tag{3.25}$$

The total flux linkage of the stator windings is

$$\lambda^s_{abc} = \lambda^s_{abc}(s) + \lambda^s_{abc}(r) \tag{3.26}$$

The procedure for finding the rotor flux linkage is very similar to finding the stator flux linkage. The flux linkage due to the rotor currents is

$$\lambda^r_{abc}(r) = \begin{bmatrix} L_{lr} + (\frac{N_r}{N_s})^2 L_{ms} & -\frac{1}{2}(\frac{N_r}{N_s})^2 L_{ms} & -\frac{1}{2}(\frac{N_r}{N_s})^2 L_{ms} \\ -\frac{1}{2}(\frac{N_r}{N_s})^2 L_{ms} & L_{lr} + (\frac{N_r}{N_s})^2 L_{ms} & -\frac{1}{2}(\frac{N_r}{N_s})^2 L_{ms} \\ -\frac{1}{2}(\frac{N_r}{N_s})^2 L_{ms} & -\frac{1}{2}(\frac{N_r}{N_s})^2 L_{ms} & L_{lr} + (\frac{N_r}{N_s})^2 L_{ms} \end{bmatrix} \begin{bmatrix} i^r_a \\ i^r_b \\ i^r_c \end{bmatrix} \tag{3.27}$$

where L_{lr} is the rotor leakage inductance

The rotor flux linkage due to stator currents is

$$\lambda_{abc}^{r}(s) = \frac{N_r}{N_s} L_{ms} \begin{bmatrix} cos\theta_r & cos(\theta_r - \frac{2\pi}{3}) & cos(\theta_r + \frac{2\pi}{3}) \\ cos(\theta_r + \frac{2\pi}{3}) & cos\theta_r & cos(\theta_r - \frac{2\pi}{3}) \\ cos(\theta_r - \frac{2\pi}{3}) & cos(\theta_r + \frac{2\pi}{3}) & cos\theta_r \end{bmatrix} \begin{bmatrix} i_a^s \\ i_b^s \\ i_c^s \end{bmatrix} \tag{3.28}$$

The summation of the two components leads to the total flux linkage of the rotor, i.e,

$$\lambda_{abc}^{r} = \lambda_{abc}^{r}(r) + \lambda_{abc}^{r}(s) \tag{3.29}$$

3.5 Park's Transformation

The time-varying inductances of stator and rotor causes difficulties in controlling the dynamic model of machine. In order to reduce the complexity of the machine, one can transfer the three coordinates into two coordinates by using the Park's transformation which was introduced by Robert H. Park in 1929. The conversion of three phase quantities into two dimensional rotating reference frame is carried out in two steps. The transformation from *abc* three coordinate system to the two coordinate stationary "$\alpha\beta$" frame is defined by Clarke's transformation. The transformation from the "$\alpha\beta$" stationary coordinate system to the "*dq*" rotating coordinate frame by rotational Park's transformation.

3.5.1 Clarke's Transformation

The *abc* three phase quantities can be transferred into stationary $\alpha\beta$ two coordinate frame using Clarke's transformation and similarly its inverse is used to transform $\alpha\beta$ two coordinate vector to *abc* three coordinate frame. f represents the any of the three vectors like current, voltage and flux. Now presenting the a, b, c coordinate frame in vector form as $\overline{f} = [f_a, f_b, f_c]^T$. The Clarke's transformation is denoted as $\overline{f}^s = f_\alpha + jf_\beta$ and is given

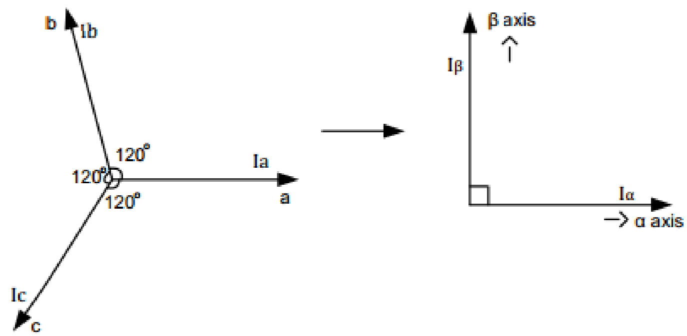

Figure 3.7: Clarke's Transformation

as follows.

$$\begin{aligned} f_\alpha + jf_\beta = \overline{f}^s =& \frac{2}{3}[f_a + e^{j\frac{2\pi}{3}} f_b + e^{j\frac{4\pi}{3}} f_c] \\ =& \frac{2}{3}(f_a - \frac{1}{2}f_b - \frac{1}{2}f_c) + j\frac{2}{3}(\frac{\sqrt{3}}{2}f_b - \frac{\sqrt{3}}{2}f_c) \end{aligned}$$

By separating real part and imaginary part, we have

$$f_\alpha = \frac{2}{3}(f_a - \frac{1}{2}f_b - \frac{1}{2}f_c) \tag{3.30}$$

$$f_\beta = \frac{2}{3}(\frac{\sqrt{3}}{2}f_b - \frac{\sqrt{3}}{2}f_c) \tag{3.31}$$

$$\begin{bmatrix} f_\alpha \\ f_\beta \\ f_0 \end{bmatrix} = \frac{2}{3} \begin{bmatrix} 1 & -\frac{1}{2} & -\frac{1}{2} \\ 0 & \frac{\sqrt{3}}{2} & -\frac{\sqrt{3}}{2} \\ \frac{1}{\sqrt{2}} & -\frac{1}{\sqrt{2}} & -\frac{1}{\sqrt{2}} \end{bmatrix} \begin{bmatrix} f_a \\ f_b \\ f_c \end{bmatrix} \tag{3.32}$$

Notice that f_0=0 due to balance three phase condition.

The Clarke's transformation and its inverse are shown in (3.33) and (3.34).

$$f_{\alpha\beta 0} = K \ \ f_{abc} \tag{3.33}$$

$$f_{abc} = K^{-1} \ \ f_{\alpha\beta 0} \tag{3.34}$$

where K and K^{-1} represents transformation matrix and its inverse.

$$K = \frac{2}{3}\begin{bmatrix} 1 & -\frac{1}{2} & -\frac{1}{2} \\ 0 & \frac{\sqrt{3}}{2} & -\frac{\sqrt{3}}{2} \\ \frac{1}{\sqrt{2}} & \frac{1}{\sqrt{2}} & \frac{1}{\sqrt{2}} \end{bmatrix} \tag{3.35}$$

$$K^{-1} = \begin{bmatrix} 1 & 0 & 1 \\ -\frac{1}{2} & \frac{\sqrt{3}}{2} & 1 \\ -\frac{1}{2} & -\frac{\sqrt{3}}{2} & 1 \end{bmatrix} \tag{3.36}$$

3.5.2 Rotational Park's Transformation

The rotational Park's transformation converts $\alpha\beta$ stationary coordinate system into dq rotating coordinate frame. The term $\overline{f}^e$ denotes the quantities in dq coordinate frame.

$$\overline{f}^e = e^{-j\theta}\overline{f}^s = f_d + jf_q$$

where, $\overline{f}^s$ denotes quantity in $\alpha\beta$ coordinate frame.

$$\begin{aligned} \overline{f}^e =& e^{-j\theta_s}[f_\alpha + jf_\beta] \\ =& (\cos\theta_s - j\sin\theta_s)(f_\alpha + jf_\beta) \\ f_d + jf_q =& f_\alpha\cos\theta_s + f_\beta\sin\theta_s - j(f_\alpha\sin\theta_s - f_\beta\cos\theta_s) \end{aligned}$$

Now, by separating the real and imaginary part and re-writing them in matrix form, we have

$$\begin{aligned} f_d =& f_\alpha\cos\theta_s + f_\beta\sin\theta_s \\ f_q =& -f_\alpha\sin\theta_s + f_\beta\cos\theta_s \end{aligned}$$

$$\begin{bmatrix} f_d \\ f_q \end{bmatrix} = \begin{bmatrix} \cos\theta_s & \sin\theta_s \\ -\sin\theta_s & \cos\theta_s \end{bmatrix} \begin{bmatrix} f_\alpha \\ f_\beta \end{bmatrix} \tag{3.37}$$

$$f_{dq} = Q\, f_{\alpha\beta} \tag{3.38}$$

$$f_{\alpha\beta} = Q^{-1}\, f_{dq} \tag{3.39}$$

where, Q and Q^{-1} represents the forward and inverse calculations of rotational Park's transformation.

$$Q = \begin{bmatrix} \cos\theta_s & \sin\theta_s \\ -\sin\theta_s & \cos\theta_s \end{bmatrix} \tag{3.40}$$

$$Q^{-1} = \begin{bmatrix} \cos\theta_s & -\sin\theta_s \\ \sin\theta_s & \cos\theta_s \end{bmatrix} \tag{3.41}$$

The total transformation from abc into dq coordinate frame is shown in Fig. 3.8.

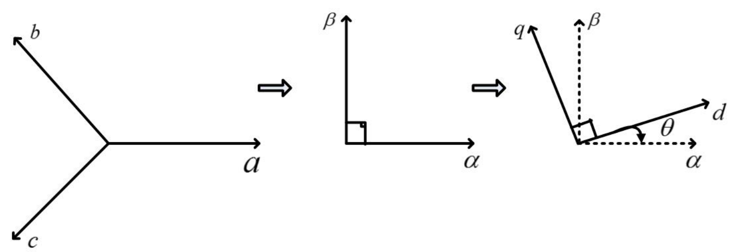

Figure 3.8: The Park's Transformation

The total Park's transformation from abc to dq coordinate frame obtained by combining (3.32) and (3.37).

$$\begin{bmatrix} f_d \\ f_q \\ f_0 \end{bmatrix} = \frac{2}{3} \begin{bmatrix} \cos\theta_s & \sin\theta_s & 0 \\ -\sin\theta_s & \cos\theta_s & 0 \\ 0 & 0 & 1 \end{bmatrix} \begin{bmatrix} 1 & -\frac{1}{2} & -\frac{1}{2} \\ 0 & \frac{\sqrt{3}}{2} & -\frac{\sqrt{3}}{2} \\ \frac{1}{\sqrt{2}} & \frac{1}{\sqrt{2}} & \frac{1}{\sqrt{2}} \end{bmatrix} \begin{bmatrix} f_a \\ f_b \\ f_c \end{bmatrix} \tag{3.42}$$

$$T(\theta) = \frac{2}{3} \begin{bmatrix} \cos\theta_s & \cos(\theta_s - \frac{2\pi}{3}) & \cos(\theta_s + \frac{2\pi}{3}) \\ -\sin\theta_s & -\sin(\theta_s - \frac{2\pi}{3}) & -\sin(\theta_s + \frac{2\pi}{3}) \\ \frac{1}{\sqrt{2}} & \frac{1}{\sqrt{2}} & \frac{1}{\sqrt{2}} \end{bmatrix} \tag{3.43}$$

The Park's transformation matrix is calculated from (3.42) and is represented by $T(\theta)$. The important property $T^{-1}(\theta_s) = \frac{3}{2}T^T(\theta_s)$ can be proved based on (3.43)

3.6 Dynamic Model of Induction Motor

The flux linkage calculated in (3.26) and (3.29) are time-varying, which causes the difficulties in controlling the dynamic model of induction machine. The complexity caused by the time-varying parameters reduced using Clarke's and Park's transformation. Assuming the turns ratio equal to 1.

From (3.24) and (3.25), the stator flux linkage (3.26) can be written as

$$\lambda^s_{abc} = L^s_{abc} i^s_{abc} + M(\theta_r).i^r_{abc} \tag{3.44}$$

where

$$L^s_{abc} = \begin{bmatrix} L_{ls} + L_{ms} & -\frac{1}{2}L_{ms} & -\frac{1}{2}L_{ms} \\ -\frac{1}{2}L_{ms} & L_{ls} + L_{ms} & -\frac{1}{2}L_{ms} \\ -\frac{1}{2}L_{ms} & -\frac{1}{2}L_{ms} & L_{ls} + L_{ms} \end{bmatrix}$$

$$M(\theta_r) = L_{ms} \begin{bmatrix} \cos(\theta_r) & \cos(\theta_r + \frac{2\pi}{3}) & \cos(\theta_r - \frac{2\pi}{3}) \\ \cos(\theta_r - \frac{2\pi}{3}) & \cos(\theta_r) & \cos(\theta_r + \frac{2\pi}{3}) \\ \cos(\theta_r + \frac{2\pi}{3}) & \cos(\theta_r - \frac{2\pi}{3}) & \cos(\theta_r) \end{bmatrix}$$

The derivations of rotor flux linkages of the equation is similar to the stator derivations except that the angle for mutual inductance is negative. The rotor flux linkage (3.29) can be written as

$$\lambda^r_{abc} = L^r_{abc} i^s_{abc} + M(-\theta_r).i^r_{abc} \tag{3.45}$$

where

$$L^r_{abc} = \begin{bmatrix} L_{lr} + L_{ms} & -\frac{1}{2}L_{ms} & -\frac{1}{2}L_{ms} \\ -\frac{1}{2}L_{ms} & L_{lr} + L_{ms} & -\frac{1}{2}L_{ms} \\ -\frac{1}{2}L_{ms} & -\frac{1}{2}L_{ms} & L_{lr} + L_{ms} \end{bmatrix}$$

$$M(\theta_r) = L_{ms}\begin{bmatrix}\cos(\theta_r) & \cos(\theta_r - \frac{2\pi}{3}) & \cos(\theta_r + \frac{2\pi}{3})\\ \cos(\theta_r + \frac{2\pi}{3}) & \cos(\theta_r) & \cos(\theta_r - \frac{2\pi}{3})\\ \cos(\theta_r - \frac{2\pi}{3}) & \cos(\theta_r + \frac{2\pi}{3}) & \cos(\theta_r)\end{bmatrix}$$

Firstly, convert all the flux linkages into the $\alpha\beta$ stationary coordinate frame using Clarke's transformation for both stator and rotor. We divide (3.44) into two parts and apply Clarke's transformation to them separately. The first part is self inductance L^s_{abc}, and the second part is mutual inductance M(θ_r).

1. **Converting first part of (3.44) $L^s_{abcs}i^s_{abc}$ into $\alpha\beta$ coordinate frame:**

   Based on Clarke's transformation, λ^s_{abc} can be written as

$$\lambda^s_{\alpha\beta} = \frac{2}{3}[\lambda^s_a(t) + e^{j\frac{2\pi}{3}}\lambda^s_b(t) + e^{j\frac{4\pi}{3}}\lambda^s_c(t)] \tag{3.46}$$

   By replacing λ^s_{abc}, with the self inductance L^s_{abc} and i_{abc} in (3.46), we get

$$\begin{aligned}\lambda^s_{\alpha\beta} = \frac{2}{3}[((L_{ls} + L_{ms})i^s_a - \frac{1}{2}L_{ms}i^s_b - \frac{1}{2}L_{ms}i^s_c)]\\ + \frac{2}{3}e^{j\frac{2\pi}{3}}(-\frac{1}{2}L_{ms}i^s_a + (L_{ls} + L_{ms})i^s_b - \frac{1}{2}L_{ms}i^s_c)\\ + \frac{2}{3}e^{j\frac{4\pi}{3}}(-\frac{1}{2}L_{ms}i^s_a - \frac{1}{2}L_{ms}i^s_b + (L_{ls} + L_{ms})i^s_c)\end{aligned} \tag{3.47}$$

   (3.47) is derived based on replacing L_{ms} with $\frac{3}{2}L_{ms} - \frac{1}{2}L_{ms}$. By rearranging the terms, we have

$$\begin{aligned}\lambda^s_{\alpha\beta} =& \frac{2}{3}[(\frac{3}{2}L_{ls} + L_{ms})(i^s_a + e^{j\frac{2\pi}{3}}i^s_b + e^{j\frac{4\pi}{3}}i^s_c)]\\ &+ \frac{2}{3}(-\frac{1}{2}L_{ms}i^s_a - \frac{1}{2}L_{ms}i^s_b - \frac{1}{2}L_{ms}i^s_c)\\ &+ \frac{2}{3}e^{j\frac{2\pi}{3}}(-\frac{1}{2}L_{ms}i^s_a - \frac{1}{2}L_{ms}i^s_b - \frac{1}{2}L_{ms}i^s_c)\\ &+ \frac{2}{3}e^{j\frac{4\pi}{3}}(-\frac{1}{2}L_{ms}i^s_a - \frac{1}{2}L_{ms}i^s_b - \frac{1}{2}L_{ms}i^s_c)\end{aligned} \tag{3.48}$$

Substituting $i_a^s + i_b^s + i_c^s = 0$ and $\frac{2}{3}(i_a^s + e^{j\frac{2\pi}{3}} i_b^s + e^{j\frac{4\pi}{3}} i_c^s) = i_{\alpha\beta}^s$ from Clarke's transformation in (3.48), we have

$$\lambda_{\alpha\beta}^s = (\frac{3}{2}L_{ms} + L_{ls}) i_{\alpha\beta}^s \tag{3.49}$$

Denote $L_s = (\frac{3}{2}L_{ms} + L_{ls})$, (3.49) becomes

$$\lambda_{\alpha\beta}^s = L_s i_{\alpha\beta}^s \tag{3.50}$$

2. **Converting second part of (3.44)** $M(\theta_r)$ i_{abc}^r **into** $\alpha\beta$ **coordinate frame:**

   Substituting the mutual inductance $M(\theta_r)$ and i_{abc}^r in the place of λ_{abc}^s in (3.46), we get

$$\begin{aligned}\lambda_{\alpha\beta}^s =& \frac{2}{3}[L_{ms}\cos(\theta_r) i_a^r + L_{ms}\cos(\theta_r + \frac{2\pi}{3}) i_b^r + L_{ms}\cos(\theta_r - \frac{2\pi}{3}) i_c^r] \\ &+ \frac{2}{3}e^{j\frac{2\pi}{3}}[L_{ms}\cos(\theta_r - \frac{2\pi}{3}) i_a^r + L_{ms}\cos(\theta_r) i_b^r + L_{ms}\cos(\theta_r + \frac{2\pi}{3}) i_c^r] \\ &+ \frac{2}{3}e^{j\frac{4\pi}{3}}[L_{ms}\cos(\theta_r + \frac{2\pi}{3}) i_a^r + L_{ms}\cos(\theta_r - \frac{2\pi}{3}) i_b^r + L_{ms}\cos(\theta_r) i_c^r]\end{aligned} \tag{3.51}$$

   Based on trigonometric function $\frac{e^{j\alpha}+e^{-j\alpha}}{2} = \cos\alpha$, we have

$$\cos(\theta_r - \frac{2\pi}{3}) = \frac{1}{2}[e^{j(\theta_r - \frac{2\pi}{3})} + e^{-j(\theta_r - \frac{2\pi}{3})}]$$

   This reduces (3.51) to

$$\lambda_{\alpha\beta}^s = \frac{1}{2}L_{ms}\frac{2}{3}[3e^{j\theta_r} i_a^r + 3e^{j\theta_r - \frac{2\pi}{3}} i_b^r + 3e^{j\theta - \frac{2\pi}{3}} i_c^r] \tag{3.52}$$

   Equivalently, we have

$$\lambda_{\alpha\beta}^s = \frac{3}{2}L_{ms}\frac{2}{3}e^{j\theta_r}(i_a^r + e^j\frac{2\pi}{3} i_b^r + e^j\frac{4\pi}{3} i_c^r) \tag{3.53}$$

   Substituting $\frac{2}{3}(i_a^r + e^{j\frac{2\pi}{3}} i_b^r + e^{j\frac{4\pi}{3}} i_c^r) = i_{\alpha\beta}^r$ into (3.53), we obtain

$$\lambda_{\alpha\beta}^s = L_m e^{j\theta_r} i_{\alpha\beta}^r \tag{3.54}$$

Denote

$$L_m = \frac{3}{2} L_{ms}$$

The combination of the first, and second part leads to the total flux linkage of stator in the $\alpha\beta$ coordinate frame. Similar procedure can be applied to determine the rotor flux linkage. The total stator and rotor flux linkages in $\alpha\beta$ coordinate frame are summarized in (3.55) and (3.56).

$$\lambda_{\alpha\beta}^s = L_s i_{\alpha\beta}^s + L_m e^{j\theta_r} i_{\alpha\beta}^r \tag{3.55}$$

$$\lambda_{\alpha\beta}^r = L_r i_{\alpha\beta}^r + L_m e^{-j\theta_r} i_{\alpha\beta}^s \tag{3.56}$$

3.7 Voltage Equations

The voltage across the stator and rotor is equal to the summation of voltage drop across their resistance and the derivation of the time varying flux linkage.

$$v_{abc}^s = r_s i_{abc}^s + \frac{d}{dt} \lambda_{abc}^s \tag{3.57}$$

$$v_{abc}^r = r_r i_{abc}^r + \frac{d}{dt} \lambda_{abc}^r \tag{3.58}$$

Converting (3.57) and (3.58) into $\alpha\beta$ stationary coordinate frame using Clarke's transformation, we have

$$v_{\alpha\beta}^s = r_s i_{\alpha\beta}^s + \frac{d}{dt} \lambda_{\alpha\beta}^s \tag{3.59}$$

$$v_{\alpha\beta}^r = r_r i_{\alpha\beta}^r + \frac{d}{dt} \lambda_{\alpha\beta}^r \tag{3.60}$$

1. The conversion of stator voltage into rotating coordinate frame

   Rotating Park's transformation is used to convert stationary coordinate frame into rotating coordinate frame, where $\overline{f}^e = e^{-j\theta_s}[f_\alpha + jf_\beta] = [f_d + jf_q]$.

   Now applying this condition to the (3.59), we have

$$v_{dq}^s = e^{-j\theta_s} v_{\alpha\beta}^s$$

$$v_{dq}^s = r_s e^{-j\theta_s} i_{\alpha\beta}^s + e^{-j\theta_s} \frac{d}{dt} \lambda_{\alpha\beta}^s$$

Since $e^{-j\theta_s} i^s_{\alpha\beta} = i^s_{dq}$, we have

$$v^s_{dq} = r_s i^s_{dq} + e^{-j\theta_s}(\frac{d}{dt}\lambda^s_{\alpha\beta})$$

Denote $e^{j\theta_s} e^{-j\theta_s} \lambda^s_{\alpha\beta} = \lambda^s_{\alpha\beta}$, and apply $e^{j\theta}.e^{-j\theta}$=1, we obtain

$$v^s_{dq} = r_s i^s_{dq} + e^{-j\theta_s}(\frac{d}{dt} e^{j\theta_s}.e^{-j\theta_s}\lambda^s_{\alpha\beta}) \tag{3.61}$$

Based on rotating Park's transformation $(e^{-j\theta_s}\lambda^s_{\alpha\beta}) = \lambda^s_{dq}$ and replace $\frac{d}{dt}\theta_s = \omega_s$ in (3.61), we get

$$\begin{aligned} v^s_{dq} =& r_s i^s_{dq} + e^{-j\theta_s}[e^{j\theta_s}.j.\omega_s.\lambda dq^s + e^{j\theta_s}\frac{d}{dt}\lambda^s_{dq}] \\ v^s_{dq} =& r_s i^s_{dq} + j\omega_s \lambda dq^s + \frac{d}{dt}\lambda^s_{dq} \end{aligned} \tag{3.62}$$

$$\begin{aligned} v^s_{dq} &= v^s_d + j v^s_q \\ i^s_{dq} &= i^s_d + j i^s_q \\ \lambda^s_{dq} &= \lambda^s_d + \lambda^s_q \end{aligned}$$

Now by separating the real and imaginary parts in (3.62), we obtain

$$v^s_d = r_s i^s_d + (-\omega_s \lambda^s_q) + \frac{d}{dt}\lambda^s_d \tag{3.63}$$

$$v^s_q = r_s i^s_q + (\omega_s \lambda^s_d) + \frac{d}{dt}\lambda^s_q \tag{3.64}$$

2. The conversion of rotor voltage into dq coordinate frame:

   Denote θ_s as the angle of stator magnetic field, with $\theta_s = \omega_s t + \theta_0$. Denote θ_r as the rotor angle, with $\theta_r = \omega_r t + \theta_{ro}$.

   Therefore, the transformation angle $\theta_s - \theta_r$ is used in rotating Park's transformation of rotor voltage. (3.60) becomes

$$
\begin{aligned}
e^{-j(\theta_s-\theta_r)}v^r_{\alpha\beta} =& e^{-j(\theta_s-\theta_r)}(r_r i^r_{\alpha\beta} + \frac{d}{dt}\lambda^r_{\alpha\beta}) \\
=& r_r i^r_{dq} + e^{-j(\theta_s-\theta_r)}\frac{d}{dt}(e^{j(\theta_s-\theta_r)}e^{-j(\theta_s-\theta_r)}\lambda_{\alpha\beta}) \\
v^r_{dq} =& r_r i^r_{dq} + j(\omega_s-\omega_r)\lambda^r_{dq} + \frac{d}{dt}\lambda^r_{dq}
\end{aligned}
$$

By separating the real and imaginary parts similar to stator voltage equations, the following equations are obtained

$$v^r_d = r_r i^r_d + \frac{d}{dt}\lambda^r_d - (\omega_s-\omega_r)\lambda^r_q \tag{3.65}$$

$$v^r_q = r_r i^r_q + \frac{d}{dt}\lambda^r_q + (\omega_s-\omega_r)\lambda^r_d \tag{3.66}$$

Since there is no supply to the rotor, (3.65) and (3.66) becomes

$$0 = r_r i^r_d + \frac{d}{dt}\lambda^r_d - (\omega_s-\omega_r)\lambda^r_q \tag{3.67}$$

$$0 = r_r i^r_q + \frac{d}{dt}\lambda^r_q + (\omega_s-\omega_r)\lambda^r_d \tag{3.68}$$

Converting flux linkages into dq coordinate frame, we have

$$\lambda^s_{dq} = e^{-j\theta_s}\lambda^s_{\alpha\beta} \tag{3.69}$$

$$\lambda^r_{dq} = e^{-j(\theta_s-\theta_r)}\lambda^r_{\alpha\beta} \tag{3.70}$$

Substituting (3.55) (3.56) into (3.69) (3.70), we have

$$
\begin{aligned}
\lambda^s_{dq} =& L_s i^s_{dq} + L_m e^{j\theta_r}.e^{-j\theta_s} i^r_{\alpha\beta} \\
\lambda^r_{dq} =& L_r i^r_{dq} + L_m e^{-j\theta_r}.e^{-j(\theta_s-\theta_r)} i^r_{\alpha\beta}
\end{aligned}
$$

Based on Park's transformation, $e^{-j\theta_s} i^r_{\alpha\beta} = i^s_{dq}$ and $e^{-j(\theta_s-\theta_r)} i^r_{\alpha\beta} = i^s_{dq}$, the following flux equations are reached.

$$\lambda^s_{dq} = L_s i^s_{dq} + L_m e^{j\theta_s} i^r_{dq} \tag{3.71}$$

$$\lambda^r_{dq} = L_r i^r_{dq} + L_m e^{-j\theta_r} i^s_{dq} \tag{3.72}$$

Now separating the real and imaginary parts in (3.71) and (3.72), we obtain

$$\lambda_d^s = L_s i_d^s + L_m i_d^r \tag{3.73}$$

$$\lambda_q^s = L_s i_q^s + L_m i_q^r \tag{3.74}$$

$$\lambda_d^r = L_r i_d^r + L_m i_d^s \tag{3.75}$$

$$\lambda_q^r = L_r i_q^r + L_m i_q^s \tag{3.76}$$

Denote, $L_s = \frac{3}{2}L_{ls} + L_m$ and $L_r = \frac{3}{2}L_{lr} + L_m$.

Substituting (3.73)-(3.76) into (3.63) (3.64) (3.67) (3.68), we have

$$v_d^s = r_s i_d^s - \omega_s(L_s i_q^s + L_m i_q^r) + \frac{d}{dt}(L_s i_d^s + L_m i_d^r) \tag{3.77}$$

$$v_q^s = r_s i_q^s + \omega_s(L_s i_d^s + L_m i_d^r) + \frac{d}{dt}(L_s i_q^s + L_m i_q^r) \tag{3.78}$$

$$0 = r_r i_d^r + \frac{d}{dt}\lambda_d^r - (\omega_s - \omega_r)(L_r i_q^r + L_m i_q^s) \tag{3.79}$$

$$0 = r_r i_q^r + \frac{d}{dt}\lambda_q^r + (\omega_s - \omega_r)(L_r i_d^r + L_m i_d^s) \tag{3.80}$$

Denote $\frac{d}{dt} = p$ and slip $\omega_{sl} = (\omega_s - \omega_r)$, (3.77)-(3.80) can be rewritten as

$$\begin{bmatrix} v_d^s \\ v_q^s \\ 0 \\ 0 \end{bmatrix} = \begin{bmatrix} r_s + pL_s & -\omega_s L_s & pL_m & -\omega_s L_m \\ \omega_s L_s & r_s + pL_s & \omega L_m & pL_m \\ pL_m & -\omega_{sl} L_m & r_r + pL_r & -\omega_{sl} L_r \\ \omega_{sl} L_m & pL_m & \omega_{sl} L_r & r_r + pL_r \end{bmatrix} \begin{bmatrix} i_d^s \\ i_q^s \\ i_d^r \\ i_q^r \end{bmatrix} \tag{3.81}$$

3.7.1 Power and Torque

The torque of the machine can be obtained by taking derivative of the electric power with respect to the angular speed.

$$T_e = \frac{dP_e}{d\omega_r} = \frac{P}{2}\frac{dP_e}{d\omega_s} \tag{3.82}$$

where ω_s is the electrical speed, ω_r is the mechanical speed P is the number of poles. The power of the rotor is zero, since there is no voltage in the rotor. The power applied to the stator is the total power input.

$$P_e = (v^s_{abc})^T i^s_{abc} \tag{3.83}$$

Based on the Park's transformation $v^s_{abc} = (T^{-1} v^s_{dqo})$ and $i^s_{abc} = (T^{-1} i^s_{dqo})$, (3.83) can be expressed as

$$\begin{aligned} P_e =& (T^{-1} v^s_{dqo})^T T^{-1} i^s_{dqo} \\ =& \frac{3}{2}(T^T v^s_{dqo})^T T^{-1} i^s_{dqo} \\ =& \frac{3}{2} v^s_{dqo} T T^{-1} i^s_{dqo} \\ =& \frac{3}{2} v^s_{dqo} i^s_{dqo} \end{aligned} \tag{3.84}$$

since $TT^{-1} = 1$ Now, substitute $(v^s_{dqo})^T = \begin{bmatrix} v^s_d & v^s_q & 0 \end{bmatrix}$ and $i^s_{dqo} = \begin{bmatrix} i^s_d \\ i^s_q \\ 0 \end{bmatrix}$ in (3.84), we have

$$P_e = \frac{3}{2}(v^s_d i^s_d + v^s_q i^s_q) \tag{3.85}$$

Now, substituting (3.81) into (3.85) we get

$$\begin{aligned} P_e =& \frac{3}{2}[(r_s + pL_s) i^s_d - \omega L_s i^s_q + pL_m i^r_d - \omega_s L_m i^r_q] i^s_d \\ &+ [\omega_s L_s i^s_d + (r_s + pL_s) i^s_q + \omega_s L_m i^r_d + pL_m i^r_q] i^s_q \end{aligned}$$

The torque of the machine can be obtained as

$$T_e = \frac{P}{2}\frac{3}{2} L_m (i^s_q i^r_d - i^s_d i^r_q) \tag{3.86}$$

The torque equation (3.86) can also be written as following

$$\begin{aligned} T_e =& \frac{P}{2}\frac{3}{2} L_m Im((i^s_d + j i^s_q) + (i^r_d + j i^r_q)) \\ T_e =& \frac{P}{2}\frac{3}{2} L_m Im(i^s_{dq} i^{r*}_{dq}) \end{aligned} \tag{3.87}$$

From (3.72), the torque equation (3.87) can be written as

$$
\begin{aligned}
T_e =& \frac{P}{2}\frac{3}{2}L_m Im[\frac{1}{L_r}(i^s_{dq}\lambda^{r*}_{dq})] \\
T_e =& \frac{P}{2}\frac{3}{2}\frac{L_m}{L_r}Im(i^s_{dq}\lambda^{r*}_{dq})
\end{aligned} \tag{3.88}
$$

Substituting $\lambda^{r*}_{dq} = \lambda^r_d - j\lambda^r_q$ and $i^s_{dq} = i^s_d + ji^s_q$ in eq (3.88), we have

$$
\begin{aligned}
T_e =& \frac{P}{2}\frac{3}{2}\frac{L_m}{L_r}Im[(i^s_d + ji^s_q)(\lambda^r_d - j\lambda^r_q)] \\
T_e =& \frac{P}{2}\frac{3}{2}\frac{L_m}{L_r}(\lambda^r_d i^s_q - \lambda^r_q i^s_d)
\end{aligned} \tag{3.89}
$$

3.8 Summary

The dynamic model of induction motor is derived in this chapter. The concept of rotating magnetic field is explained, and the equivalent circuit of induction motor is illustrated. Park's and Clarke's transformations are used to convert *abc* quantities frame to *dq* frame. The dynamic model of induction motor in *dq* coordinate frame is presented.

CHAPTER 4

POWER ELECTRONICS

4.1 Insulated Gate Bipolar Transistor

Insulated gate bipolar transistors are also called IGBT for short. It makes use of MOSFET input characteristics and BJT output characteristics. Now-days they are primarily used as high efficiency and fast switching devices in power electronic devices such as inverters, converters, PWM and power supplies.

4.1.1 Construction and Operation

The simple equivalent circuit model of IGBT in Fig. 4.1 shows a MOSFET driving the NPN and PNP transistors. The PNP collector is connected to the base of NPN, and the collector of NPN is connected to the base of PNP. The resistor R_B is used to prevent the IGBT latch up by shorting of the base-emitter of the NPN transistor. The IGBT circuit symbol is shown in Fig. 4.2. The operation modes of IGBT are achieved by

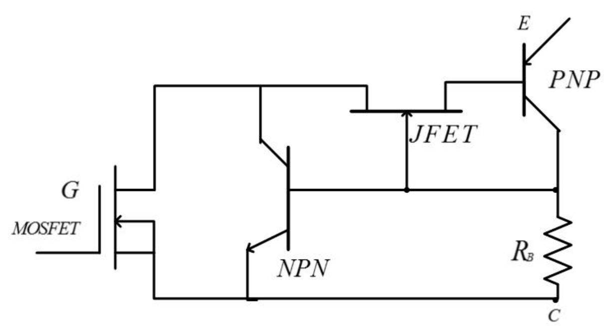

Figure 4.1: The Equivalent Circuit of IGBT

applying a positive voltage across the gate to turn emitter on. We can turn off the IGBT by applying a voltage less than the V_{th}. IGBT's are classified into two types based on the construction. If they consist of N+ buffer layer then, it is called punch through IGBT (PT IGBT), otherwise they are called non-PT IGBT(NPT IGBT). The addition of N+

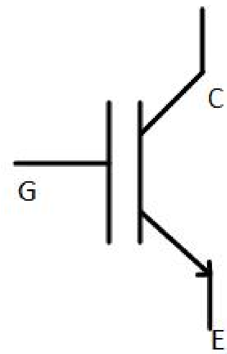

Figure 4.2: IGBT Symbol

buffer layer improves the performance of the device by reducing the time to turn off in reverse blocking mode of IGBT.

4.1.2 Characteristics

The output characteristics of IGBT is shown in Fig. 4.3. The collector current is measured as a function of collector-emitter voltage V_{CE} at different V_{GE} values. The transfer characteristics of IGBT are obtained by changing collector current I_c with respect to the V_{GE} at different temperatures. The ratio of current to the voltage leads to the

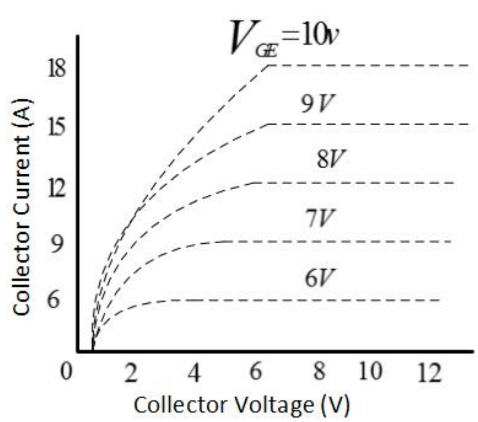

Figure 4.3: The Output Characteristics of IGBT

transconductance g_f at a given temperature.

$$g_f = \frac{dIc}{dV_{GE}} \tag{4.1}$$

A large g_f is designed to obtain high current capability at low gate voltage. The device must be operated in a safe region in motor control applications.

4.2 Inverters

Inverters are converters used to convert the DC voltage to the AC voltage of required magnitude and frequency. They can get a fixed or variable output voltage for a fixed or variable frequency. The output can be varied by changing the input supply or by varying the gain of the inverter. The gain of the inverter can be changed using pulse width modulation control for the inverter. The inverters mainly used in industrial applications, such as variable speed AC motor drives, transportation, uninterrupted power supplies, etc. For high power applications, the harmonics can be reduced by using high-speed semiconductor devices such as IGBT, IGCT. The inverters can be classified into two types: current source inverters and voltage source inverters.

4.2.1 Current Source Inverter(CSI)

In current source inverter, the output current is constant and independent of the load applied to the inverter. The CSI operation can be achieved by keeping a series of inductor on the input side. The inductor provides constant input dc current source. The example of a three-phase current source inverter is shown in Fig. 4.4.

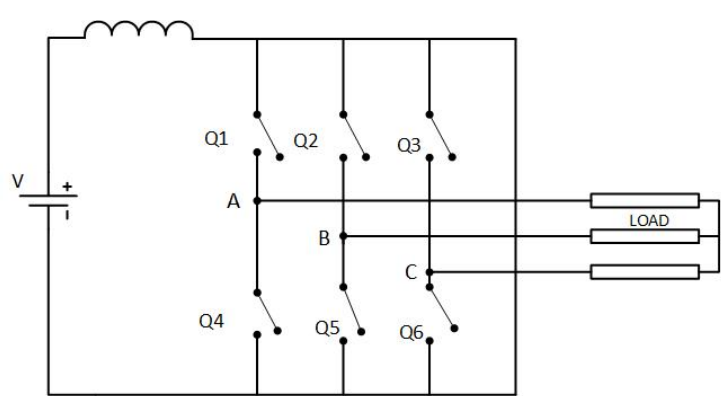

Figure 4.4: Current Source Inverter

4.2.2 Voltage Source Inverter(VSI)

The function VSI is to convert fixed DC voltage to a variable AC voltage. Depending upon the type of applications one can use single or three phase inverters. The three-phase inverter can be constructed by using three single phase half bridge inverter in parallel. The other way to get three phase output is by using six semiconductor switches such as MOSFET, IGBT, IGCT, etc.

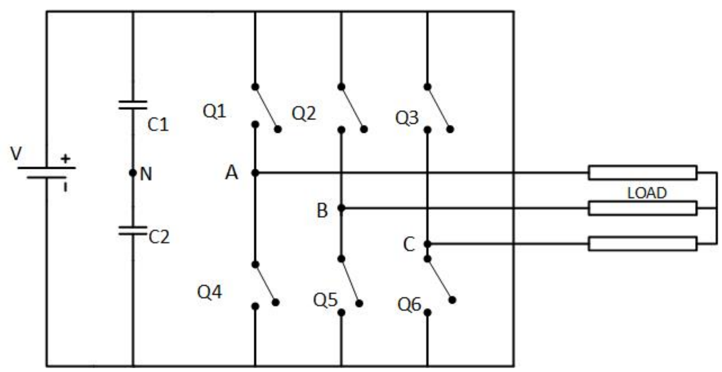

Figure 4.5: Voltage Source Inverter

The Fig 4.5 shows a simple circuit of the three phase VSI consisting of six switches and two capacitors. The capacitors are placed to provide a neutral point N and each capacitor keeps half of the voltage Vd. The inverter may be connected to a Y or delta connected load. IGBTs are used in place of switches in our thesis. Two popular type of VSI's: 120^0 conduction and 180^0 modes VSI's are introduced below:

4.2.3 180^0 *Conduction Mode*

In 180^0 conduction, each switch conducts for 180^0. As seen from the Fig 4.5, there are six switches. Consider, Q1 and Q4 as leg A, Q2 and Q5 as leg B, Q3 and Q6 as leg C. The switches are turned on for a time interval of 180^0. Therefore, Q1 is turned on for 180^0 and Q4 for next 180^0 of a cycle. The upper group switches conduct for an interval of 120^0. It means if Q1 is turned at t=0, then Q2 should turn on 120^0 and Q3 start to turn on at 240^0. This type of firing the pulses to get a phase shift of 120^0 for three output voltages. The Fig 4.6 shows the duration of each switch and the sequence of the switches turning on . It shows for every 60^0, three switches are conducting two from the lower group and one from the upper group, or one from the lower group and two from the upper group. If switch Q1 is closed, the terminal A of first leg is connected to the positive of input DC voltage. If the other switch of the same leg Q4 is turned on, the terminal point A is connected to the negative DC voltage. The two switches of the same leg should not turn on at the same time, in order to avoid short circuit. The similar approach is carried out for the remaining legs.

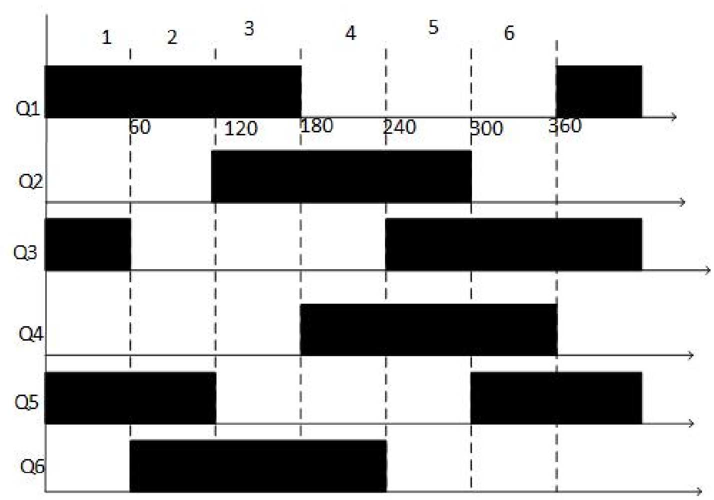

Figure 4.6: The Operation of Switches Per Cycle

There are six states of operation for each cycle, and each state is operated for 60^0 as shown in the Fig. 4.6. In mode 1, the switches Q1, Q3 and Q5 are on. The balanced load Z is considered, and the voltage across the each load is determined using Fig 4.7. The voltage across the switch Q1, Q3 is $\frac{V}{3}$ and the voltage along Q5 is -$\frac{2V}{3}$ based on Fig 4.7. Only state one and state two are shown in the figure. The Fig 4.6 shows the active switches in each mode over a cycle. The determination of voltages for remaining states are similar to these two states. The calculated voltages are phase voltages.

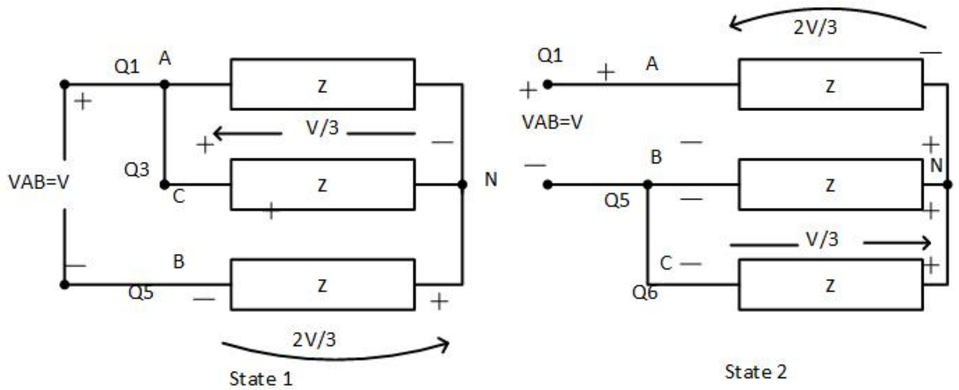

Figure 4.7: The Calculation of Voltages in State 1 and 2

The line to line voltages can be obtained from phase voltages using (4.2), (4.3) and (4.4)

$$V_{ab} = V_{an} - V_{bn} \tag{4.2}$$

$$V_{bc} = V_{bn} - V_{cn} \tag{4.3}$$

$$V_{ca} = V_{cn} - V_{an} \tag{4.4}$$

The output phase and line voltages over a cycle are shown in the Fig 4.5. The IGBT is

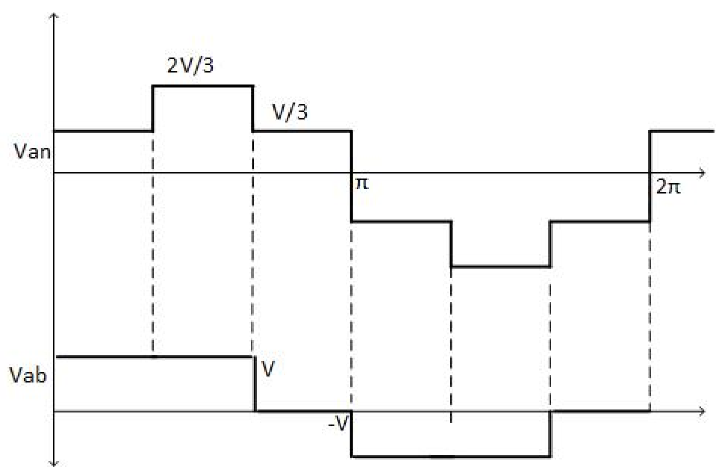

Figure 4.8: The Output Phase and Line Voltages of 180 Conduction

used in the place of switches. Diodes are connected in parallel to the IGBT to provide a path for adverse currents, when the switch is turned off.

4.3 Simulation of 180^0 Conduction Mode

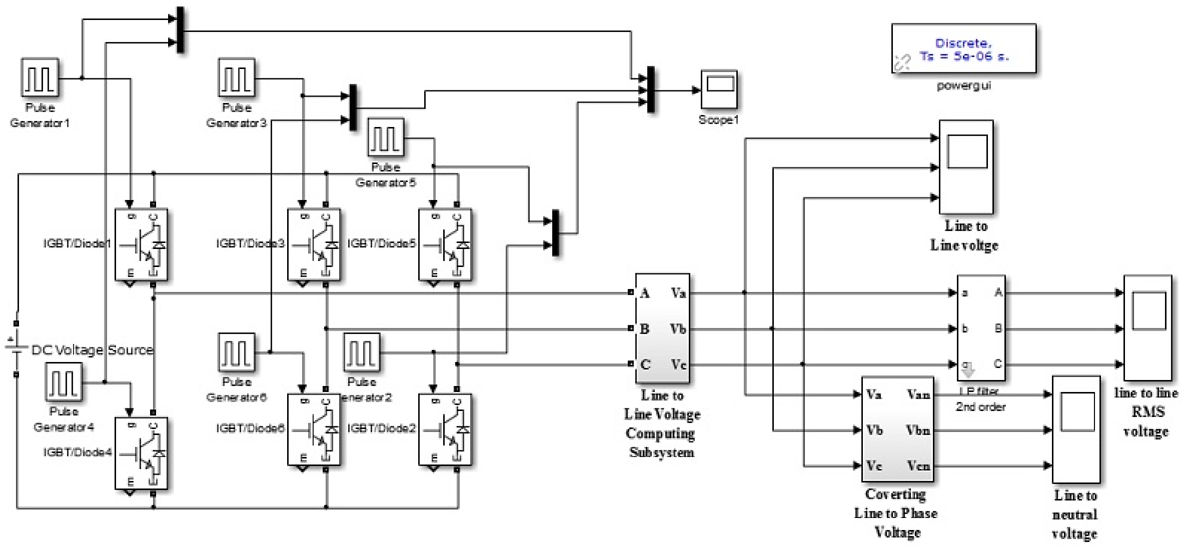

Figure 4.9: Simulink of 180^0 Conduction

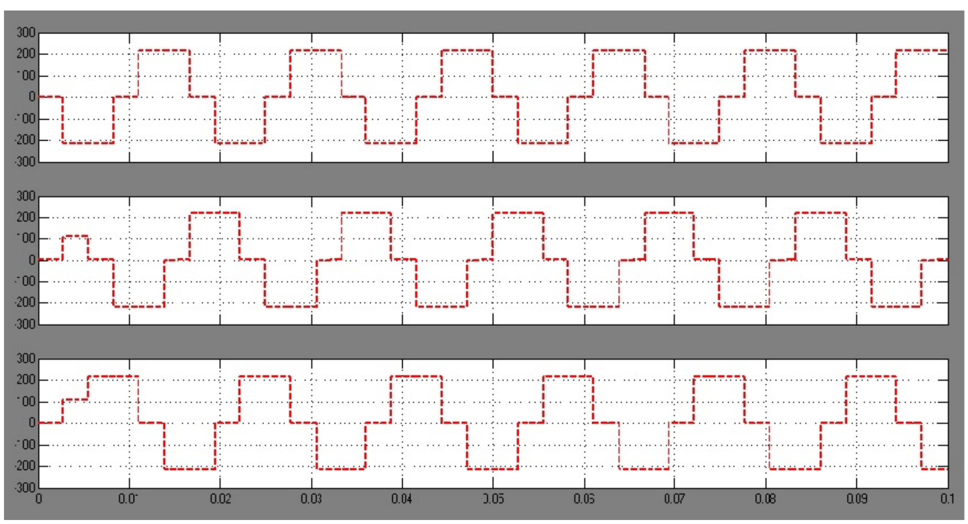

Figure 4.10: 180^0 Line to Line Voltage Conduction

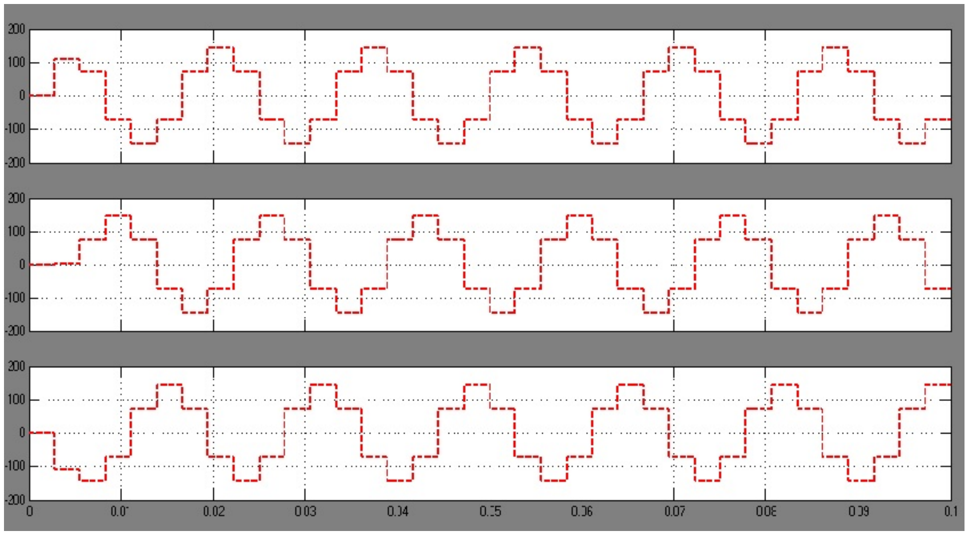

Figure 4.11: 180^0 Phase Voltage Conduction

4.3.1 120^0 *Conduction Mode*

In 120^0 conduction mode, each switch operates for 120^0 conduction cycle. The operation of the switches is similar to 180^0 mode, however, in every state only switches are on at the same time. The pair in each leg are turned on for a time interval of 120^0. For example, if Q1 is turned on for 120^0, then Q4 is turned on at 180^0 and conducts for 120^0. That means during 60^0 interval, both Q1 and Q4 are off. The operation is similar for the remaining legs. The upper group switches conducts at an interval of 120^0 similar to case in 180^0 conduction mode. The operation of lower group switches is similar to upper group switches, which leads to a phase shift of 120^0. The operation of switches of one cycle is shown in Fig 4.12.

Similar to 180^0, it requires six states over one cycle and each state conducts for 60^0. In every state, only two switches are conducting, depending upon the on and off states of switches the respective voltages are determined using the following Fig 4.13 and Fig 4.14.

For example, in the state 1 Q1 and Q5 are on, and in state 2 Q1 and Q6 are on. The terminal voltages are determined based on the state of its operation. If Q1 is on, the

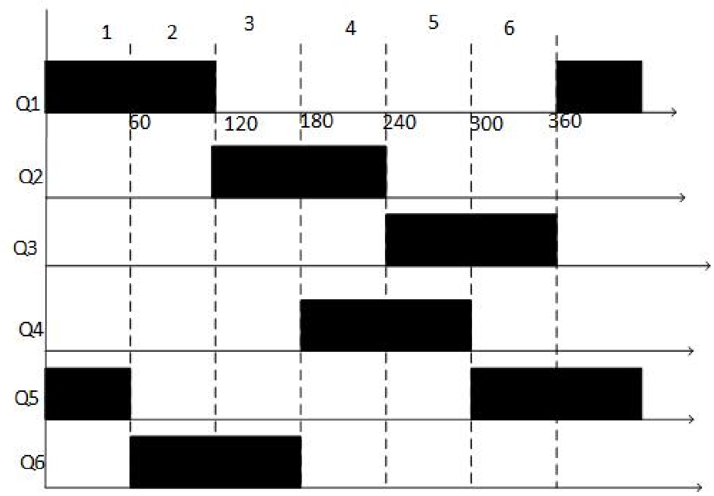

Figure 4.12: Operation of Switches Over a Cycle

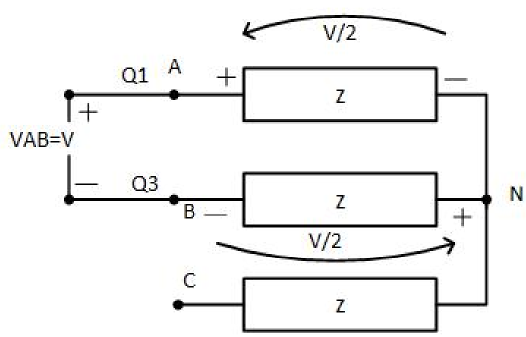

Figure 4.13: State 1

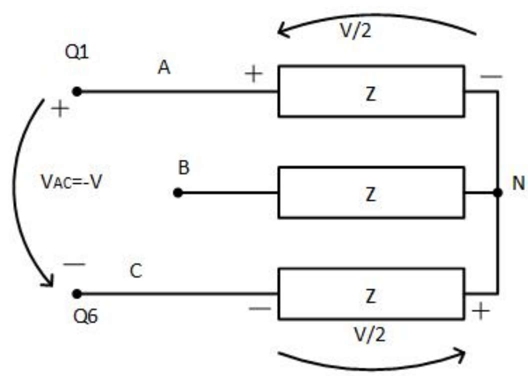

Figure 4.14: State 2

switch is connected to the positive terminal of supply, therefore point A, the voltage is V/2. Q5 is connected to the negative terminal of the supply, therefore point B, the voltage is -V/2. Similarly, the operation of state 2 is shown in Fig 4.14. The phase and line voltages per phase are shown in the Fig 4.15.

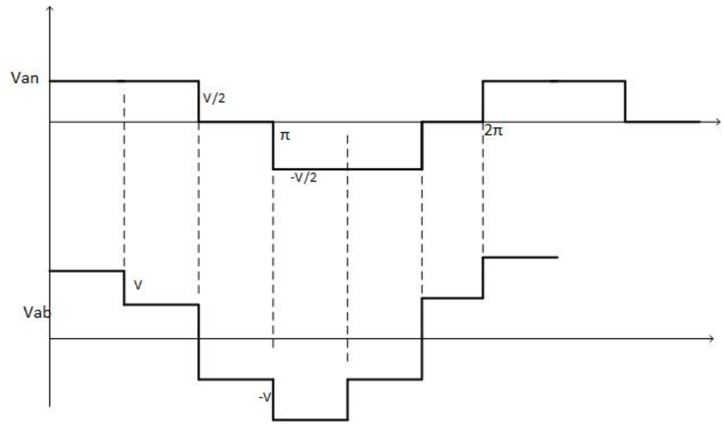

Figure 4.15: The Output Line and Phase Voltages of 120^0 Conduction

4.4 Simulation of 120^0 Conduction Mode

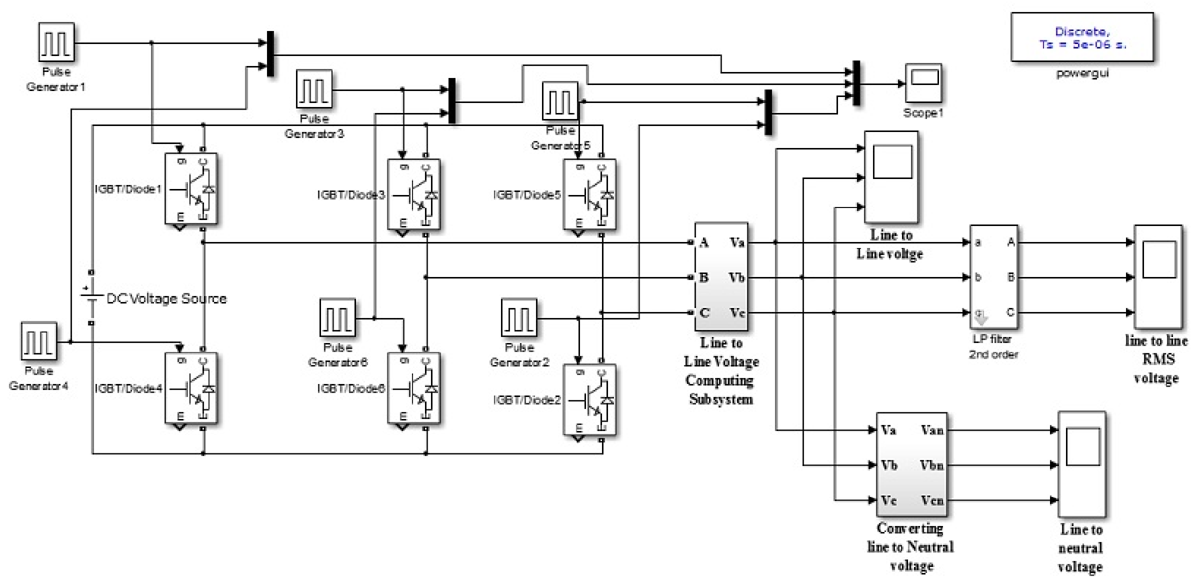

Figure 4.16: Simulink of 120^0 Conduction

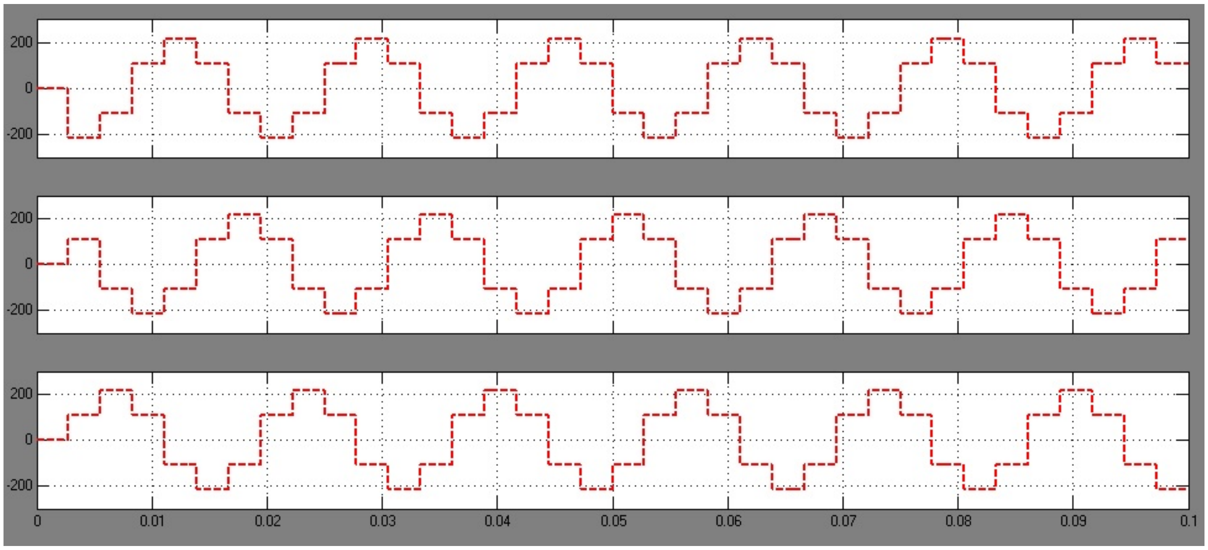

Figure 4.17: 120^0 Line to Line Voltage Conduction

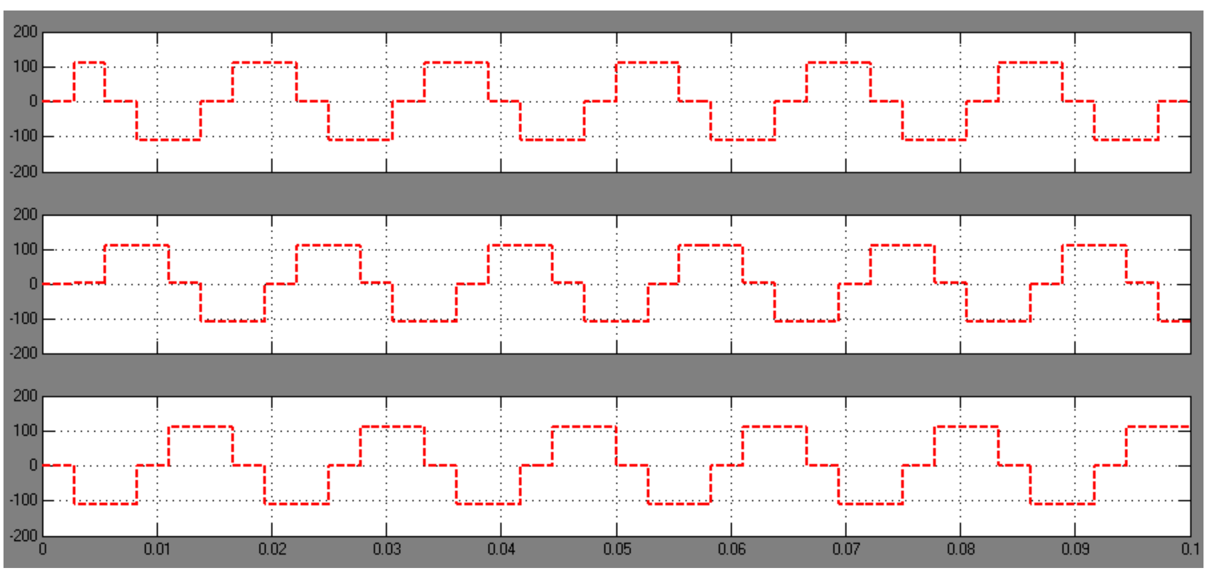

Figure 4.18: 120^0 Phase Voltage Conduction

In order to control the output voltage, we need to change the gain by using PWM control. The two main PWM controls which are widely used in the industry are sinusoidal PWM and space vector PWM.

4.5 Space Vector PWM

The output of three-phase voltage source inverter can be shaped using the Space Vector PWM technique. When top switches are on, i.e., S1, S3 or S5 is 1, the corresponding lower switches S4, S6 or S7 are off. The output voltages are determined by selecting the on and off modes of the three upper switches and therefore, the total possible number of combinations are 2^3.

The relation between the phase voltage and line to line voltages to the switching states of the two lever inverter are given as follows

$$\begin{bmatrix} v_{ab} \\ v_{bc} \\ v_{ca} \end{bmatrix} = V_{dc} \begin{bmatrix} 1 & -1 & 0 \\ 0 & 1 & -1 \\ -1 & 0 & 1 \end{bmatrix} \begin{bmatrix} a \\ b \\ c \end{bmatrix} \tag{4.5}$$

$$\begin{bmatrix} v_a \\ v_b \\ v_c \end{bmatrix} = \frac{1}{3} V_{dc} \begin{bmatrix} 2 & -1 & -1 \\ -1 & 2 & -1 \\ -1 & -1 & 2 \end{bmatrix} \begin{bmatrix} a \\ b \\ c \end{bmatrix} \tag{4.6}$$

Based on the on and off states of upper switches, we can show the lower switches on and off-states, because they act complimentary to the upper switches. The output line to line and phase voltage are summarized in Table 4.1.

Implementation of Space Vector PWM

The output voltages of inverter are balanced three phase voltages. The three phase balanced voltages from the inverter output differ from each other by 120^0. The three

Table 4.1: Switching Pattern of Two Level VSI and Voltage Space Vectors w.r.t V_{dc}

V	S1	S3	S5	v_{an}	v_{bn}	v_{cn}	v_{ab}	v_{bc}	v_{ca}
V0	0	0	0	0	0	0	0	0	0
V1	1	0	0	$\frac{2}{3}$	$-\frac{1}{3}$	$-\frac{1}{3}$	1	0	-1
V2	1	1	0	$\frac{1}{3}$	$\frac{1}{3}$	$-\frac{2}{3}$	0	1	-1
V3	0	1	0	$-\frac{1}{3}$	$\frac{2}{3}$	$-\frac{1}{3}$	-1	1	0
V4	0	1	1	$-\frac{2}{3}$	$\frac{1}{3}$	$\frac{1}{3}$	-1	0	1
V5	0	0	1	$-\frac{1}{3}$	$-\frac{1}{3}$	$\frac{2}{3}$	0	-1	1
V6	1	0	1	$\frac{1}{3}$	$-\frac{2}{3}$	$\frac{1}{3}$	1	-1	0
V7	1	1	1	0	0	0	0	0	0

phase voltages in the a, b, c coordinate frame are transfmored to the stationary two coordinate frame using Clark's transformation. The voltage equations in the three-phase are transferred to the $\alpha\beta$ coordinate frame as shown in the Fig. 4.19.

$$v_{\alpha\beta 0} = \; f_0 \, v_{abc}$$

We can neglect the zero component in the two stationary coordinate frame, because the sum of three phase balanced voltages is equal to zero.

$$V_a + V_b + V_c = 0 \tag{4.7}$$

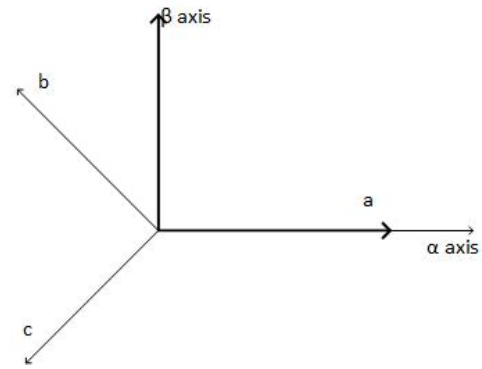

Figure 4.19: Clarke's Transformation

$$\begin{bmatrix} v_\alpha \\ v_\beta \end{bmatrix} = \frac{2}{3} \begin{bmatrix} 1 & -\frac{1}{2} & -\frac{1}{2} \\ 0 & \frac{\sqrt{3}}{2} & -\frac{\sqrt{3}}{2} \end{bmatrix} \begin{bmatrix} v_a \\ v_b \\ v_c \end{bmatrix} \tag{4.8}$$

After the transformation into $\alpha\beta$ coordinate frame, from total eight combinations of turn off and on of switches, we get six non-zero vectors and two zero vectors. The six non-zero vectors supply power to the load and the zero vectors supply no power to the load. The eight vectors are considered to be the space vectors and formed the six vertices's of a hexagon. The remaining two zero vectors are located at the origin as shown in Fig 4.18. The same transformation can be applied to get the reference voltage vector V_{ref} in $\alpha\beta$ plane. Now obtain the reference voltage from those eight space vectors. The eight space vectors are considered to be stationary vectors and the only vector rotates in space is V_{ref} with an angular velocity ω =$2\pi f$, where f is the inverter frequency.

1. Determine $V_\alpha, V_\beta, V_{ref}$, and the vector reference angle ($\alpha°$)

   Based on $V_\alpha, V_\beta, V_{ref}$, and angle ($\alpha$) can be determined as follows:

$$\begin{bmatrix} v_\alpha \\ v_\beta \end{bmatrix} = \frac{2}{3} \begin{bmatrix} 1 & -\frac{1}{2} & -\frac{1}{2} \\ 0 & \frac{\sqrt{3}}{2} & -\frac{\sqrt{3}}{2} \end{bmatrix} \begin{bmatrix} v_a \\ v_b \\ v_c \end{bmatrix}$$

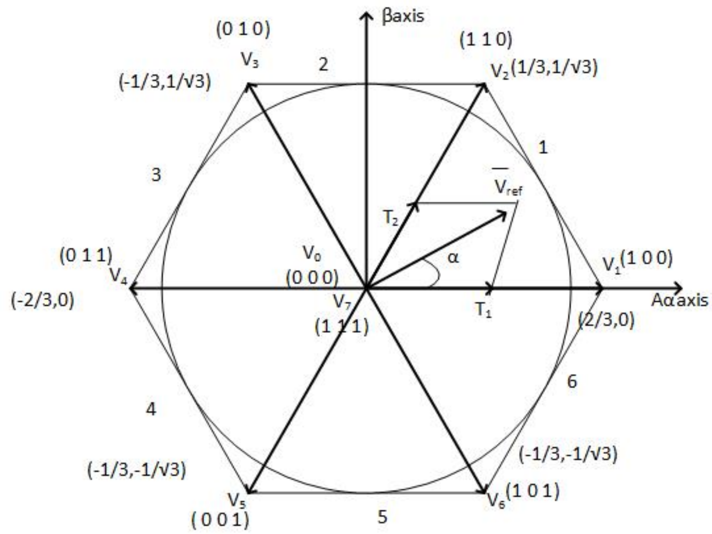

Figure 4.20: Hexagon Representation of Space Vectors

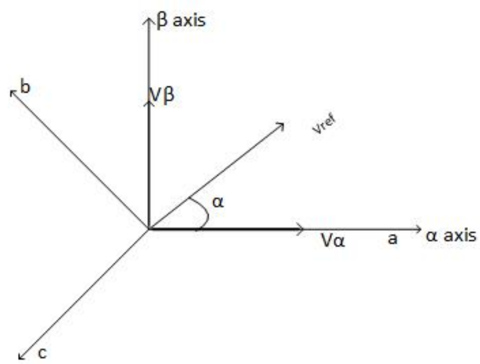

Figure 4.21: The V_{ref} in α β axis

$$|V_{ref}| = \sqrt{v_\alpha^2 \ + \ v_\beta^2} \tag{4.9}$$

$$\alpha^\circ \ = \ \tan^{-1}\frac{v_\alpha}{v_\beta} \ = \ \omega t = 2\pi f t \tag{4.10}$$

where f is the fundamental frequency of the desired output voltage.

2. Determine time duration of T_1, T_2 and T_0

   Considering V_{ref} is in Sector 1, and it can be synthesized by vectors adjacent to it in that sector. The time duration of the V_{ref} is based on the following principle:

The product of reference voltage and its sampling time period equal to the sum of voltages multiplied by their time interval of space vectors in chosen sector [6]. In the

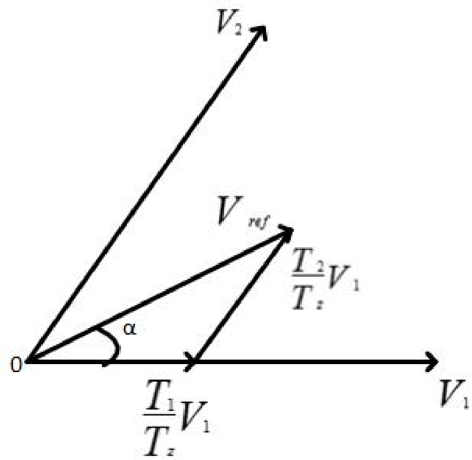

Figure 4.22: The Reference Voltage in Sector 1

Fig 4.19, we showed the corresponding space vectors and respective time duration.

- Switching time duration in sector 1

$$\int_{T_0}^{T_z} \overline{V}_{ref} = \int_{T_0}^{T_1} V_1 \, dt \ + \int_{T_1}^{T_1+T_2} \overline{V}_2 \, dt \ + \int_{T_1+T_2}^{T_z} \overline{V}_0 \, dt$$

$$T_z \ = \ T_1 \ + \ T_2 \ + \ T_0 \tag{4.11}$$

where T_1, T_2 and T_0 are the switching time of $\overline{V}_1, \overline{V}_2$ and $\overline{V}_0$, respectively. T_z is switching period ($2T_z = T_s = \frac{1}{f_s}$). T_s, and f_s are the sampling time and frequency. From above equation, we obtain

$$T_z \, \overline{V}_{ref} \ = \ T_1 \, \overline{V}_1 \ + \ T_2 \, \overline{V}_2 + \ T_0 \, \overline{V}_0 \tag{4.12}$$

However, $\overline{V}_0$ applies a zero voltage to the output load, so the equation becomes

$$T_z \, \overline{V}_{ref} \ = \ T_1 \, \overline{V}_1 \ + \ T_2 \, \overline{V}_2 \tag{4.13}$$

Now, substituting the value of $\overline{V}_1$ and $\overline{V}_2$ from Tab.4.1

$$T_z\,|\overline{V}_{ref}|\begin{bmatrix}\cos\alpha\\ \\ \sin\alpha\end{bmatrix} \;=\; T_1\,\frac{2}{3}\,V_{dc}\begin{bmatrix}1\\ \\ 0\end{bmatrix} \;+\; T_2\,\frac{2}{3}\,V_{dc}\begin{bmatrix}\cos\frac{\pi}{3}\\ \\ \sin\frac{\pi}{3}\end{bmatrix}$$

$$T_2 \;=\; T_z\,\frac{3}{2}\,\frac{|\overline{V}_{ref}|}{V_{dc}}\,\frac{\sin\alpha}{\sin\frac{\pi}{3}}$$

$$T_2 \;=\; T_z\;a\,\frac{\sin\alpha}{\sin\frac{\pi}{3}} \tag{4.14}$$

$$T_1 \;=\; T_z\,\frac{3}{2}\,\frac{|\overline{V}_{ref}|}{V_{dc}}\,\frac{\sin(\frac{\pi}{3}-\alpha)}{\sin\frac{\pi}{3}}$$

$$T_1 \;=\; T_z\;a\,\frac{\sin(\frac{\pi}{3}-\alpha)}{\sin\frac{\pi}{3}} \tag{4.15}$$

The angle between any two adjacent sides of hexagon is 60^0, therefore ($0° \;\leqslant\; \alpha \;\leqslant\; 60°$) in sector one, and a is the modulation index, $a = \frac{|\overline{V}_{ref}|}{\frac{2}{3}\,V_{dc}}$.

- Switching time duration in arbitrary sector

The time duration in the other sectors can be calculated by substituting $\alpha = \alpha - (n-1)\frac{\pi}{3}$, where n is the sector number which is from 1 to 6

$$T_1 \;=\; T_z\,\frac{3}{2}\,\frac{|\overline{V}_{ref}|}{V_{dc}}\,\frac{\sin(\frac{\pi}{3}-(\alpha-(n-1)\frac{\pi}{3}))}{\sin\frac{\pi}{3}}$$

$$=\;\frac{\sqrt{3}\,T_z\,|\overline{V}_{ref}|}{V_{dc}}\,\sin\,(\frac{n}{3}\,\pi\;-\;\alpha)$$

then

$$T_1 = \frac{\sqrt{3}\,T_z\,|\overline{V}_{ref}|}{V_{dc}}\,\{\sin\,(n\frac{\pi}{3})\;\cos(\alpha)\;-\;\cos(n\frac{\pi}{3})\;\sin(\alpha)\} \tag{4.16}$$

$$T_2 \;=\; T_z\,\frac{3}{2}\,\frac{|\overline{V}_{ref}|}{V_{dc}}\,\frac{\sin(\alpha-(n-1)\frac{\pi}{3})}{\sin\frac{\pi}{3}}$$

$$=\;\frac{\sqrt{3}\,T_z\,|\overline{V}_{ref}|}{V_{dc}}\,\sin\,(\;\alpha\;+\;(n-1)\frac{\pi}{3})$$

$$T_2 = \frac{\sqrt{3}\,T_z\,|\overline{V}_{ref}|}{V_{dc}}\,\{\cos((n-1)\frac{\pi}{3})\sin(\alpha)+\cos(\alpha)\sin((n-1)\frac{\pi}{3})\} \tag{4.17}$$

$$T_0 \;=\; T_z \;-(\;T_1\;+\;T_2\;) \tag{4.18}$$

- To find sector number:

To get sector number, n, first of all, we use angle α from the step 1 considering one cycle(0,2π), we divide angle by 2π and take the remaining angle for one cycle. In the hexagon each sector is multiple of $\pi/3$, so we divide new angle by $\pi/3$ and round that reminder to a less integer. The sector number can find by adding one to the integer .

For example, let $\alpha = 300°$:

$$\begin{aligned} remain &= rem(\frac{300°}{360°}) \\ &= 140° \\ n &= 1\;+fix(\frac{40°}{60°}) = 1\;+\;fix(0.66667) \\ &= 1\;+\;0 = 1 \end{aligned}$$

Therefore sector number is 1.

- Switching sequence:

The switching sequence of any type must satisfy the following two conditions, In order to minimize the device switching frequency. a. The change of switching state from one to another involves only two switches in the same inverter leg, if either one of them on, then the other must be off, to reduce the switching frequency.

b. The moving of V_{ref} from one sector to the next requires no or minimum number of switchings in order to reduce the switching losses [6].

Table 4.2: Calculation of Switching Time at each Sector

Sector	Upper Group Switches (S_1, S_3, S_5)	Lower Group Switches (S_4, S_6, S_2)
1	$S_1 = T_1 + T_2 + T_0/2$ $S_3 = T_2 + T_0/2$ $S_5 = T_0/2$	$S_4 = T_0/2$ $S_6 = T_1 + T_0/2$ $S_2 = T_1 + T_2 + T_0/2$
2	$S_1 = T_1 + T_0/2$ $S_3 = T_1 + T_2 + T_0/2$ $S_5 = T_0/2$	$S_4 = T_2 + T_0/2$ $S_6 = T_0/2$ $S_2 = T_1 + T_2 + T_0/2$
3	$S_1 = T_0/2$ $S_3 = T_1 + T_2 + T_0/2$ $S_5 = T_2 + T_0/2$	$S_4 = T_1 + T_2 + T_0/2$ $S_6 = T_0/2$ $S_2 = T_1 + T_0/2$
4	$S_1 = T_0/2$ $S_3 = T_1 + T_0/2$ $S_5 = T_1 + T_2 + T_0/2$	$S_4 = T_1 + T_2 + T_0/2$ $S_6 = T_2 + T_0/2$ $S_2 = T_0/2$
5	$S_1 = T_2 + T_0/2$ $S_3 = T_0/2$ $S_5 = T_1 + T_2 + T_0/2$	$S_4 = T_1 + T_0/2$ $S_6 = T_1 + T_2 + T_0/2$ $S_2 = T_0/2$
6	$S_1 = T_1 + T_2 + T_0/2$ $S_3 = T_0/2$ $S_5 = T_1 + T_0/2$	$S_4 = T_0/2$ $S_6 = T_1 + T_2 + T_0/2$ $S_2 = T_2 + T_0/2$

4.5.1 Simulation of Space Vector PWM

The simulation results of SVPWM are summarized in Fig. **??** to Fig. **??**.

4.6 Summary

The operation and characteristics of IGBT are explained in the chapter. The conduction modes of 120^0 and 180^0 voltage source inverters (VSI) are studied. The concept and design of Space Vector PWM considered in this chapter. The Space Vector PWM is simulated using Matlab/Simulink. The results show that the SV PWM method produces less harmonic distortion in the ouput waveform.

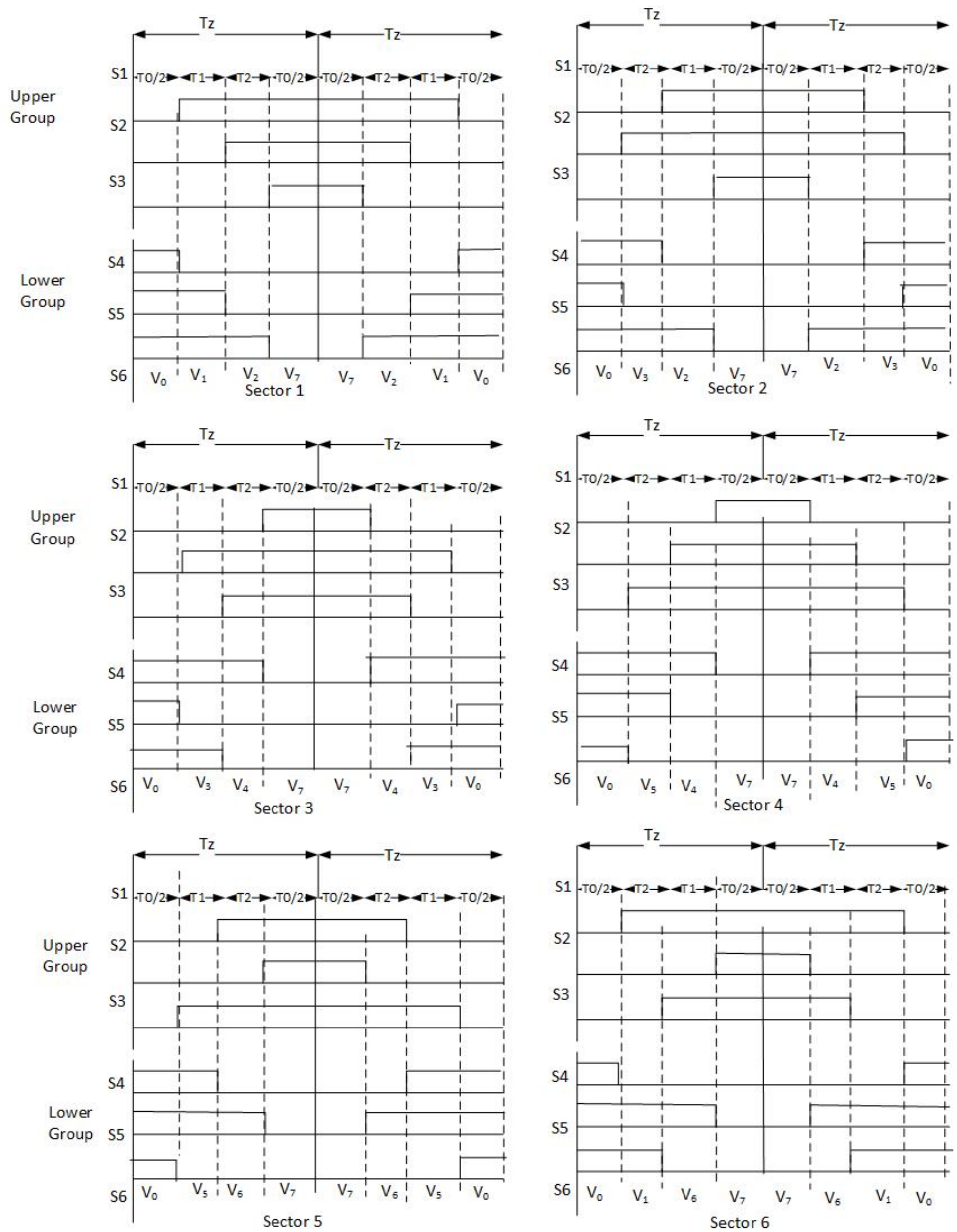

Figure 4.23: The Switching Pattern of SVPWM at each Sector

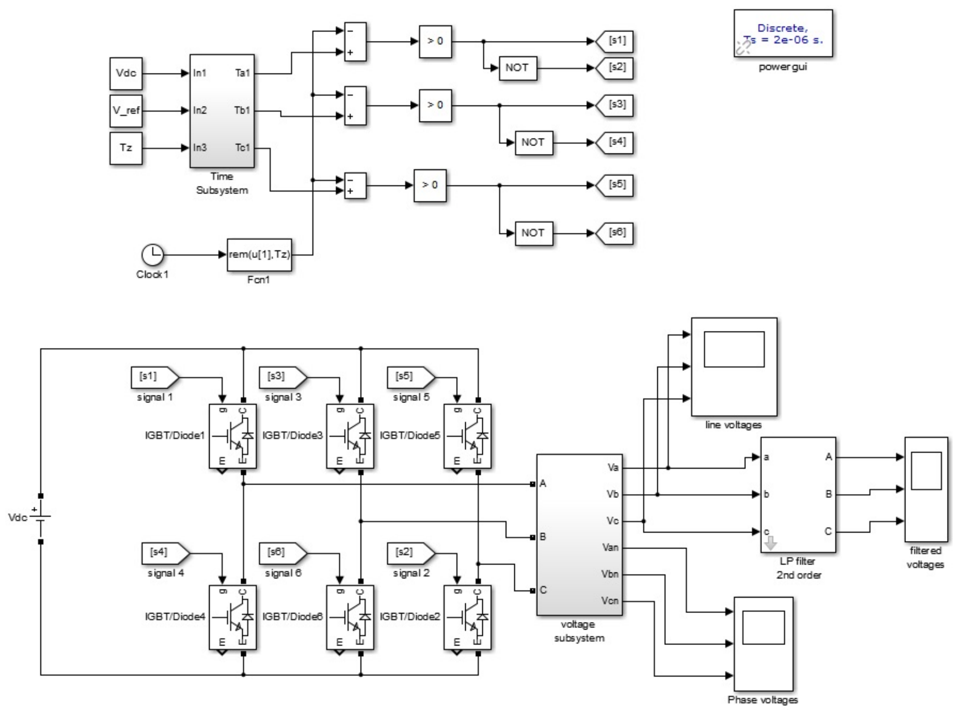

Figure 4.24: Simulation of Space Vector PWM for VSI

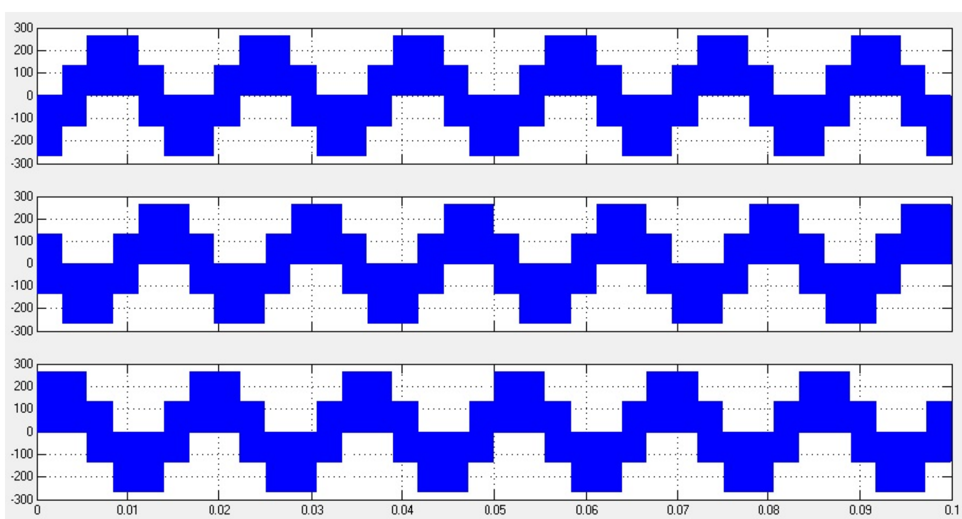

Figure 4.25: The Output Line to Neutral Voltage

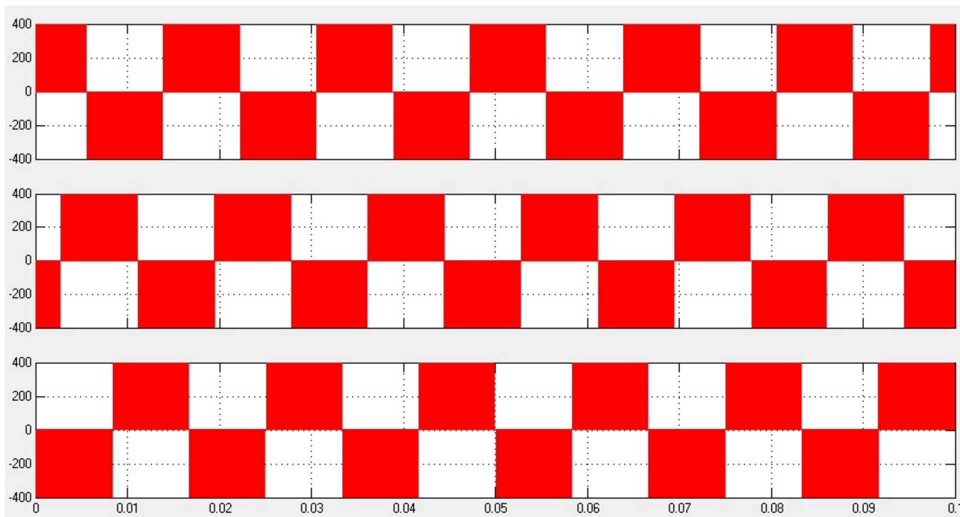

Figure 4.26: The Output Line to Line Voltage

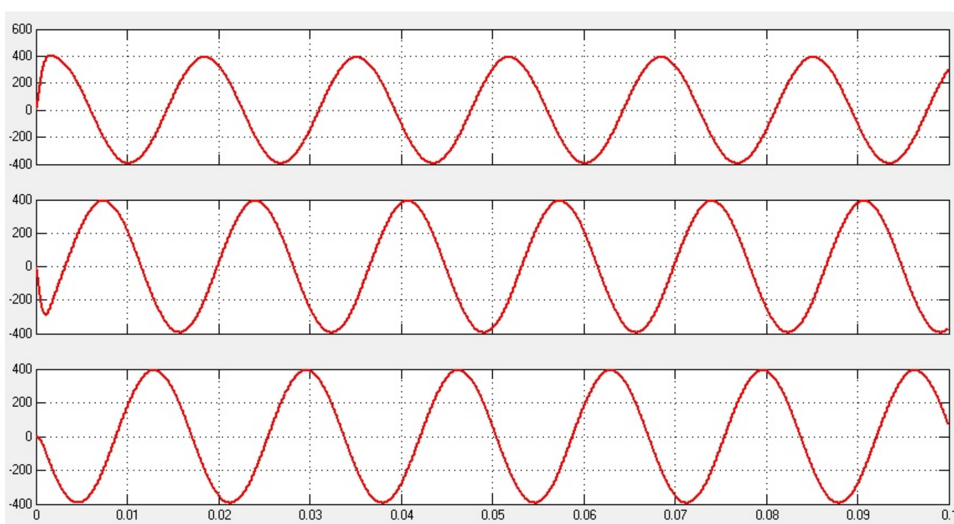

Figure 4.27: The Output Filtered Voltage

CHAPTER 5

FIELD ORIENTED CONTROL

5.1 Introduction

The DC motors have been widely used in variable speed control applications. In DC drives, the torque and flux are decoupled and can be controlled by the armature and field current. However, DC machines have many disadvantages, such as sparks, commutator and brushes wear out, difficulty to maintain, etc. The field oriented control of induction motor was first developed by F.Blaschke in 1972. The development in power electronic devices and microprocessors make the AC machines speed control available and overcome the disadvantages of DC machines like high cost, commutator and brushes problems. Initially, the speed control of induction machine are performed by changing the voltage and frequency and keeping the V/f ratio constant e.t.c. These type of controlling methods are called the scalar control methods. The high performance of field oriented control drives outperform the scalar control method due to the following advantages:

- full torque control capability at low speed
- better dynamic behavior
- higher efficiency
- operating point in a wide range of speed
- decoupled torque and flux control
- four quadrant operation

As we apply the concept of DC motor control to the AC machines, let's see how torque is produced and flux is controlled in the DC motors. A simple construction of DC motor is shown in the Fig 5.1. The field winding are represented by a pair of magnetic poles, which are stationary and are considered as stator of the machine. The flux produced by field winding aligned along direct axis of the stator. The armature winding is considered to be the rotor. The current flowing in the rotor is always aligned along the quadrature axis because commutator and brushes keep it along the q-axis. The torque is proportional to the cross product of current i_a and flux λ_f. The current and flux are along the two axis of coordinate system, which means they always perpendicular to each other and produces maximum torque all the time. The torque equation of DC motor which can be used as

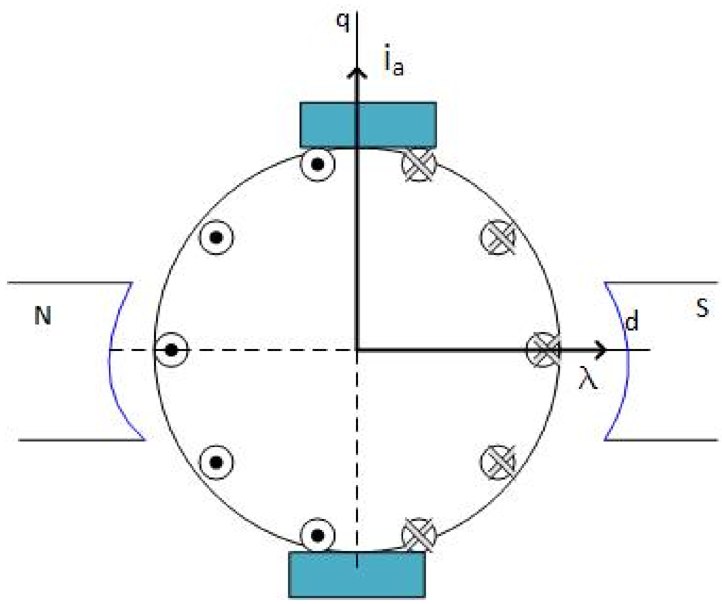

Figure 5.1: A Simple Representation of DC Motor

reference for field oriented control is

$$\tau_m = K_T \lambda_f i_a \tag{5.1}$$

where K_T is torque constant

5.1.1 Model of field oriented control

The DC machine control approach to AC Drives is not easier, because the orientation of stator and rotor fluxes are not held orthogonal and vary with the operating conditions[18].

To obtain like DC machine control one need to align stator currents with respect to the rotor flux to get independently controlled torque and flux. This type of control achieved, Firstly, by converting AC motor dynamics into dq synchronous frame under certain conditions. Secondly, by aligning the flux of the machine to the reference frame. Depending upon the alignment of flux, the system categorized into two different schemes. If the reference frame is aligned to the stator field then it is called as stator field oriented control and if it is to the rotor flux then referred as rotor filed oriented scheme [1]. The decoupled control can be achieved by rotor field oriented control like in separately excited DC machine. However, calculation of the rotor flux is carried in two different ways. If it is measured directly by using sensors, then it is called direct Field Oriented Control (DFOC). If the measurement from slip that is calculated from dynamic model of induction motor, then it is called indirect Field Oriented Control (IFOC). The simple implementation and more reliability makes IFOC widely used in industries.

Direct field oriented control In direct field oriented scheme, the rotor flux measures from hall effect sensors. Therefore, the rotor angle can calculate from rotor flux by the equation

$$\theta = \tan^{-1} \frac{\lambda_{dr}^{s}}{\lambda_{qr}^{s}} \tag{5.2}$$

The installation of flux sensors is difficult due to limitations of air gap space, armature reaction, noise, etc. Due to these limitations the rotor flux is calculated indirectly from stator currents that are measured using current sensors.

Indirect field oriented control In this method, we have two different approaches of measuring rotor flux angle. The first one is by calculating the rotor flux equations indirectly by using the stator flux and currents, and the second is from slip information ω_{sl}. Let us see how we proceed to the rotor flux equations from the stator currents and fluxes. The current sensors are used to measure the stator currents, and fluxes can be obtained using

(5.3) and (5.4).

$$\lambda_d^s = \int_0^t (v_d^s - r_s i_d^s) dt \tag{5.3}$$

$$\lambda_q^s = \int_0^t (v_q^s - r_s i_q^s) dt \tag{5.4}$$

The equations from (3.73) to (3.76) represents the stator flux and rotor flux in synchronous rotating frame. Now converting them into $\alpha\beta$ stationary coordinate frame by multiplying with $e^{j\theta}$, we obtain

$$\lambda_\alpha^s = L_s i_\alpha^s + L_m i_\alpha^r \tag{5.5}$$

$$\lambda_\beta^s = L_s i_\beta^s + L_m i_\beta^r \tag{5.6}$$

$$\lambda_\alpha^r = L_r i_\alpha^r + L_m i_\alpha^s \tag{5.7}$$

$$\lambda_\beta^r = L_r i_\beta^r + L_m i_\beta^s \tag{5.8}$$

Now we substitute the i_α^r, i_β^r taken from (5.5) and (5.6) in (5.7) and (5.8) we get

$$\lambda_\alpha^r = \frac{L_r(\lambda_\alpha^s - L_s i_\alpha^s)}{L_m} + L_m i_\alpha^s = \frac{(L_m^2 - L_s L_r) i_\alpha^s + L_r \lambda_d^s}{L_m}$$

$$\lambda_\beta^r = \frac{L_r(\lambda_\beta^s - L_s i_\beta^s)}{L_m} + L_m i_\beta^s = \frac{(L_m^2 - L_s L_r) i_\beta^s + L_r \lambda_\beta^s}{L_m}$$

$$\sigma = 1 - \frac{L_m}{L_s L_r} \tag{5.9}$$

After rearranging the terms and substituting terms in (5.9), the two equations can be written as:

$$\lambda_\alpha^r = \frac{L_r}{L_m}(\lambda_\alpha^s - \sigma L_s i_\alpha^s), \tag{5.10}$$

$$\lambda_\beta^r = \frac{L_r}{L_m}(\lambda_\beta^s - \sigma L_s i_\beta^s) \tag{5.11}$$

Now, substituting the stator currents measured from sensors and fluxes from (5.3) and (5.4) in above equations, we get rotor flux equations. From (5.10) and (5.11), the rotor flux angle can be obtained. However, this method is not suitable when a DC offset is present.

The second method of calculating rotor flux angle, which is from slip information. From (3.67) and (3.68), we know

$$0 = r_r i_d^r + p\lambda_d^r - (\omega - \omega_r)\lambda_q^r$$
$$0 = r_r i_q^r + p\lambda_q^r + (\omega - \omega_r)\lambda_d^r$$

Now applying λ_q^r=0 and $p\lambda_q^r = 0$, The rotor equations become

$$0 = r_r i_d^r + p\lambda_d^r \tag{5.12}$$
$$0 = r_r i_q^r + (\omega - \omega_r)\lambda_d^r \tag{5.13}$$

From (3.75) we know λ_d^r and substituting that in (5.12), we get

$$\begin{aligned} 0 =& r_r i_d^r + p(L_r i_d^r + L_m i_d^s) \\ =& (r_r + L_r p) i_d^r + pL_m i_d^s \\ i_d^r =& \frac{-pL_m i_d^s}{(r_r + L_r p)} \end{aligned}$$

Again by substituting i_d^r in the (3.75), i.e, λ_d^r becomes

$$\begin{aligned} \lambda_d^r =& L_r \frac{-pL_m i_d^s}{(r_r + L_r p)} + L_m i_d^s \\ =& i_d^s [L_m - \frac{L_r L_m}{r_r + L_r p} p] \end{aligned}$$

After canceling the respective terms the rotor flux along the direct axis, λ_d^r can be written as

$$\lambda_d^r = \frac{L_m}{1 + pT_r} i_d^s \tag{5.14}$$

where T_r is rotor time constant

$$T_r = \frac{L_r}{r_r} \tag{5.15}$$

In the steady state

$$\lambda_d^r = L_m i_d^s \tag{5.16}$$

Since $\lambda_q^r = 0$, (3.76) can be written as $i_q^r = -\frac{L_m i_q^s}{L_r}$, substituting this equation in (5.13), we obtain the slip speed information

$$slip\_speed = \omega_{sl} = \omega_s - \omega_r = \frac{r_r}{L_r}\frac{L_m}{\lambda_d^r} i_q^s \tag{5.17}$$

Now, adding obtained slip speed to the rotor shaft speed, we get synchronous speed of the machine. The rotor flux angle can be measured by integrating the synchronous speed which is shown in (5.18).

$$\theta_s = \int_0^t \omega_e dt = \int_0^t (\omega_{sl} + \omega_r) dt \tag{5.18}$$

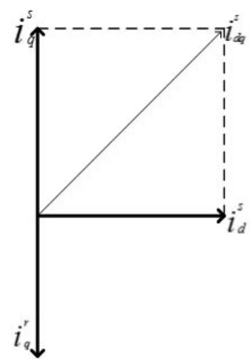

Figure 5.2: The Vector Representation of Rotor Field Oriented Scheme

- From $\lambda_d^r = \frac{L_m}{1+pT_r} i_d^s$, we find that i_d^s is used to generate rotor flux.

- Comparing the (3.75) and (5.16), we obtain i_d^r=0

- From (5.17), i_q^s is proportional to the slip

- From $i_q^r = -\frac{L_m}{L_r} i_q^s$, we find i_q^r nullifies flux caused by i_q^s.

The $\lambda_q^r = 0$ reduces the torque equation (3.86) to follow the equation, which is similar to the DC machine

$$T_e = \frac{3}{2}\frac{P}{2}\frac{L_m}{L_r}(\lambda_d^r i_q^s) \tag{5.19}$$

Based on the filed oriented control method, we have the flux along the direct axis and current along the quadrature axis, which is similar to the DC machine. Based on (5.16) and (5.17), the rotor flux along the direct axis is proportional to the i_d^s and the current i_q^s along the quadrature axis is proportional slip. The two currents i_d^s, i_q^s are to be used for the control of Induction machine.

5.2 The Basic Scheme for Field Oriented Control of Induction Motor

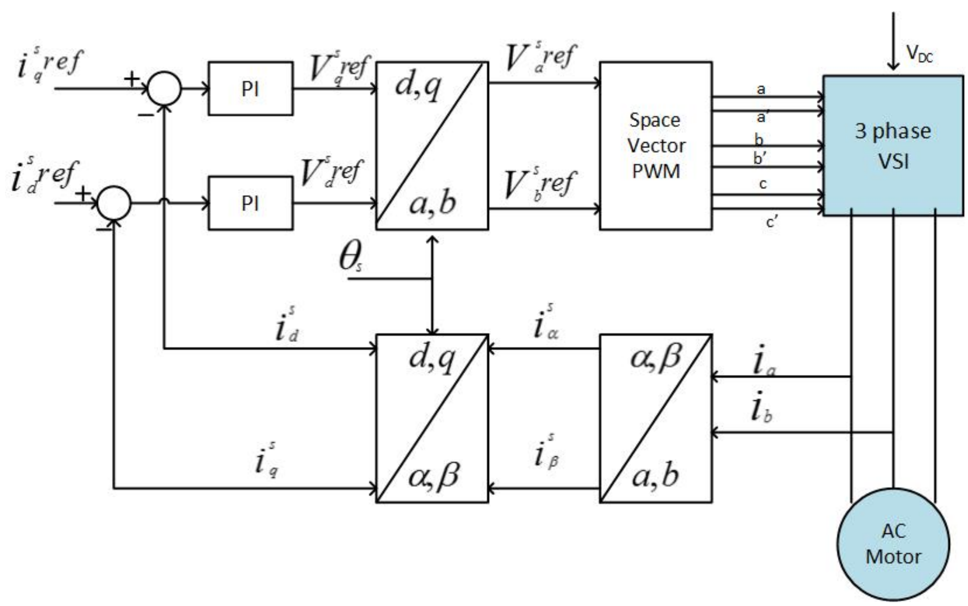

Figure 5.3: The Basic Scheme of Field Oriented Control

Fig 5.3 explains the basic scheme of speed control with FOC. Firstly, it measure the two input currents of the motor. These input currents are converted to stationary coordinate frame using Clarke's transformation module. The currents in the stationary frame are converted to rotating frame using Park's transformation module. These currents are compared to the reference currents, and the resulting error is passed through the current controllers. The output of current controllers, which are in dq coordinate frame, are converted into $\alpha\beta$ coordinate frame using inverse rotating Park's transformation module. These are input to the Space Vector PWM module. The output of Space Vector PWM module operates the gating signal of the three phase inverter. The Clarke and Park Transformation modules require the rotor flux position which is the key factor in controlling the machine. The calculation of rotor flux position is mentioned in direct and indirect rotor field oriented scheme.

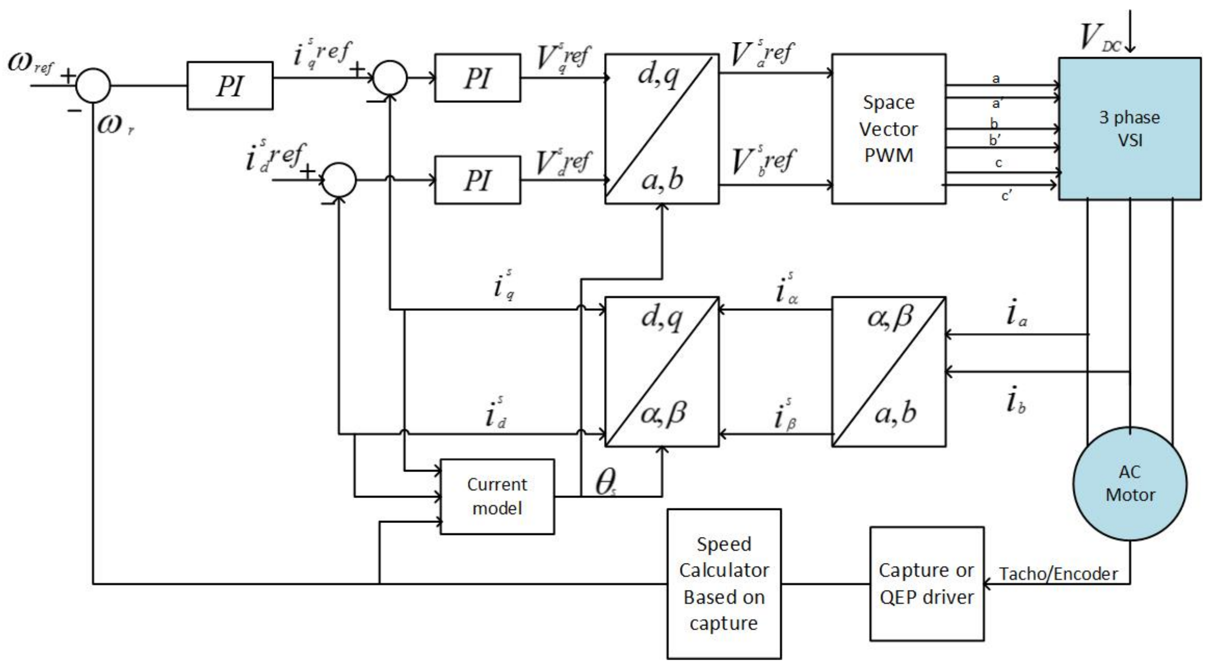

Figure 5.4: Block Diagram of Indirect Rotor Field Oriented scheme

5.2.1 Rotor Field Oriented Scheme

From (3.75) and (3.76), we get

$$i_d^r = \frac{1}{L_r}(\lambda_d^r - L_m i_d^s) \tag{5.20}$$

$$i_q^r = \frac{1}{L_r}(\lambda_q^r - L_m i_q^s) \tag{5.21}$$

substituting (5.20) and (5.21) into the system model (3.81)

$$v_d^s = (r_s + p\sigma L_s)i_d^s + \frac{L_m}{L_r}p\lambda_d^r - \omega[\frac{L_m}{L_r}\lambda_q^r + L_s\sigma i_q^s] \tag{5.22}$$

$$v_q^s = (r_s + p\sigma L_s)i_q^s + \frac{L_m}{L_r}p\lambda_q^r + \omega[\frac{L_m}{L_r}\lambda_d^r + L_s\sigma i_d^s] \tag{5.23}$$

where

$$\sigma = (1 - \frac{L_m}{L_s L_r})$$

The field-oriented control can be achieved by aligning the rotor flux along the direct axis, i.e., $\lambda_q^r = 0$, and $p\lambda_q^r = 0$. Therefore, (5.22) and (5.23) are reduced to

$$v_d^s = (r_s + p\sigma L_s)i_d^s - \omega_e\sigma L_s i_q^s + \frac{L_m}{L_r}p\lambda_d^r \tag{5.24}$$

$$v_q^s = (r_s + p\sigma L_s)i_q^s + \omega_e\sigma L_s i_d^s + \omega_e\frac{L_m}{L_r}p\lambda_d^r \tag{5.25}$$

The torque equation (3.88) reduced to

$$T_e = \frac{3}{2}\frac{p}{2}\frac{L_m}{L_r}\lambda_d^r i_q^s \tag{5.26}$$

Applying the Laplace transformation for above two voltage equations and considering the steady state condition p$\lambda_d^r = 0$

$$i_d^s = \frac{\frac{1}{L_s\sigma}}{s + \frac{r_s}{L_s\sigma}}v_d^s + \frac{\omega_e}{s + \frac{r_s}{L_s\sigma}}i_q^s \tag{5.27}$$

$$i_q^s = \frac{\frac{1}{L_s\sigma}}{s + \frac{r_s}{L_s\sigma}}v_q^s - \frac{\omega_e}{s + \frac{r_s}{L_s\sigma}}i_d^s - \frac{\frac{L_m}{L_r L_m \sigma}}{s + \frac{r_s}{L_s\sigma}}\omega_e\lambda_d^r. \tag{5.28}$$

Neglecting the r_s term and considering p λ_d^r=0 for the steady state condition, we reach the following conditions:

$$L_s\sigma\frac{d}{dt}i_d^s = u_d^s + \omega_e L_s\sigma i_q^s \tag{5.29}$$

$$L_s\sigma\frac{d}{dt}i_q^s = u_q^s - \omega_e L_s\sigma i_d^s - \omega_e\frac{L_m}{L_r}\lambda_d^r \tag{5.30}$$

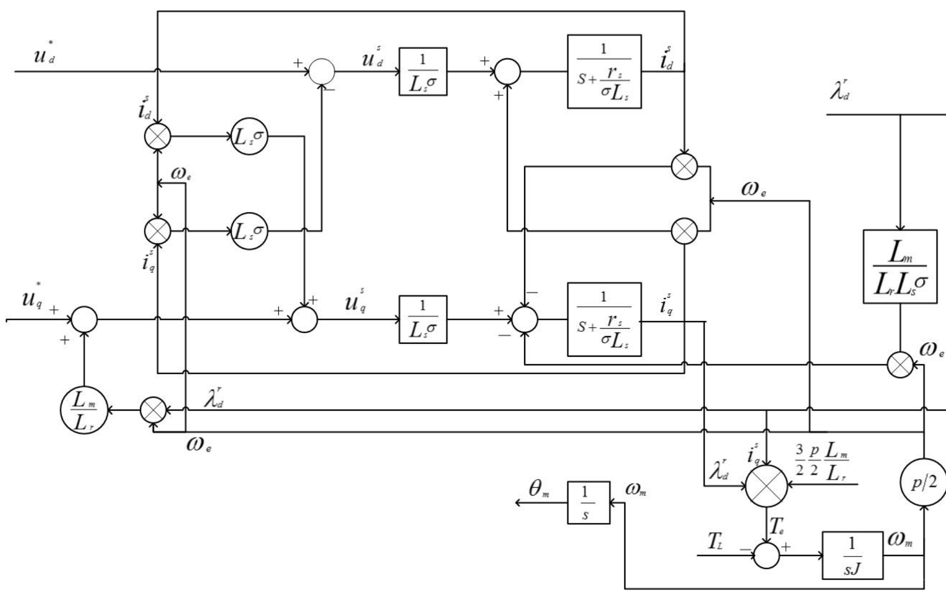

Figure 5.5: The Block Diagram of Feed Forward Control

From (5.24) and (5.25), we find $\omega_e L_s \sigma i_q^s$ and $-\omega_e L_s \sigma i_d^s$, are cross-coupling current terms of d-axis and q-axis. In order to decouple the coupling terms, the feed-forward control as shown in the Fig. 5.5.

Equate right hand side of equations (5.29) and (5.30) with u_d^* and u_q^*, we have

$$u_d^* = u_d^s + \omega_e L_s \sigma i_q^s \tag{5.31}$$

$$u_q^* = u_q^s - \omega_e L_s \sigma i_d^s - \omega_e \frac{L_m}{L_r} \lambda_d^r \tag{5.32}$$

By applying the Laplace transformation, we have the plant transfer function $G_i(s)$ for the current control as

$$G_i(s) = \frac{i_d^s}{u_d^*} = \frac{1}{L_s \sigma s} \tag{5.33}$$

$$G_i(s) = \frac{i_q^s}{u_q^*} = \frac{1}{L_s \sigma s} \tag{5.34}$$

where

$$\sigma = 1 - \frac{L_m}{L_s L_r} \tag{5.35}$$

5.2.2 PI Current Controller Design

Let's consider the PI controller given below

$$R_i(s) = k_p(1 + \frac{1}{sT_i}) \tag{5.36}$$

where

$$T_i = \frac{k_p}{k_i}$$

We design current controller based on frequency response method using the phase and gain margin. Let us choose the crossover frequency $\omega_c = \frac{2\pi f_s}{10}$, where f_s is the switching frequency of the inverter and phase margin PM=60^0, i.e.

$$|G_{i,o}(j\omega_c)| = 1 \tag{5.37}$$

$$arg(G_{i,o}(j\omega_c)) = -\frac{2\pi}{3} \tag{5.38}$$

The transfer function of the plant to be controlled is (5.33) for direct and (5.34) for quadrature axis current control, respectively. The overall schematic for current control loop is shown in Fig .5.6. From the Fig 5.3, the open loop transfer function is

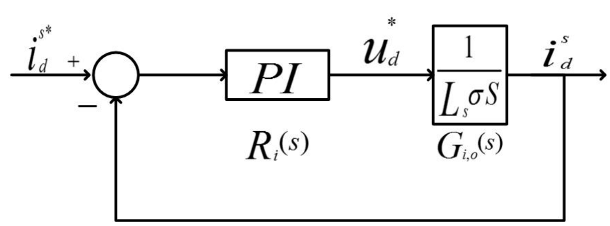

Figure 5.6: The Block Diagram of Direct Axis Current Control

$$G_{i,o} = R_i(s)G_i(s) = \frac{K_p^i}{L_s\sigma T_i^i}\frac{1}{s^2}(1 + sT_i^i)$$

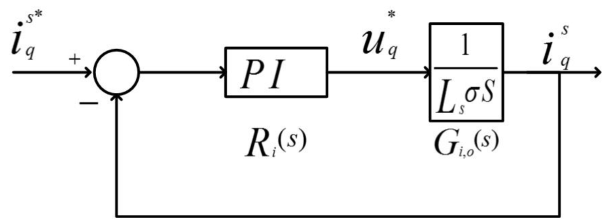

Figure 5.7: The Block Diagram of the Quadrature Axis Current Control

where K_p^i and T_i^i are the corresponding K_p and T_i parameters for current PI controller. Applying the phase margin condition (5.38) of $G_{i,o}$ we have

$$\begin{aligned} arg(G_{i,o}(j\omega_c)) =& tan^{-1}\frac{\omega_c T_i^i}{1} - \pi \\ =& tan^{-1}(\omega_c T_i^i) - \pi = -\frac{2\pi}{3} \end{aligned} \tag{5.39}$$

Therefore, the T_i^i value can be obtained from (5.39).

Applying the magnitude condition (5.38) of $G_{i,o}$ and substituting T_i^i value, we get K_p^i.

$$\begin{aligned} G_{i,o}(j\omega_c) =& \frac{K_p^i}{L_s \sigma T_i^i}\frac{1}{\omega_c^2}\sqrt{1 + (\omega_c T_i^i)^2} = 1 \\ K_p^i =& \frac{L_s \sigma T_i^i \omega_c^2}{\sqrt{1 + (\omega_c T_i^i)^2}} \end{aligned} \tag{5.40}$$

Therefore, based on the calculated T_i^i and K_p^i values, we obtain K_i^i from

$$K_i^i = \frac{K_p^i}{T_i^i} \tag{5.41}$$

The closed loop transfer function can be obtained based on the open loop transfer function $G_{i,o}$, as follows

$$G_{i,c} = \frac{G_{i,o}}{1 + G_{i,o}} = \frac{1 + sT_i^i}{1 + sT_i^i + s^2\frac{T_i^i \sigma L_s}{K_p^i}} \tag{5.42}$$

The Bode plot of closed-loop system is shown in Fig.5.8, and the step response is shown in Fig.5.9.

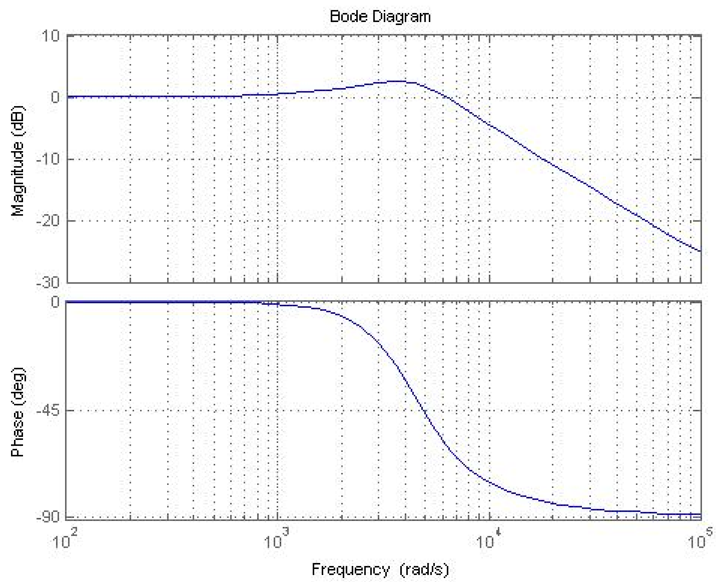

Figure 5.8: The Bode Plot of the Closed loop system

5.2.3 PI Speed Controller Design

In this section, we design the K_p^w and K_i^w values for the speed controller using symmetrical optimum method, which guarantees the maximum phase margin. First, notice that (5.42) is a second-order system, we need to approximate it by a simplified first-order transfer function. That significantly simplified the speed controller design as follows.

$$G_{i,c}(s) = G_{i,sim}(s) = \frac{1}{1 + \frac{s}{\omega_g}} \tag{5.43}$$

where $\omega_g = \frac{1}{T_g}$

Since the magnitude of closed loop transfer function decreased by 20 dB/decade for high frequencies, the cut-off frequency of low pass filter can be determined easily. First, the frequency ω_1, is chosen as ten times the switching frequency:

$$\omega_1 = 10 \cdot f_s \cdot 2\pi \tag{5.44}$$

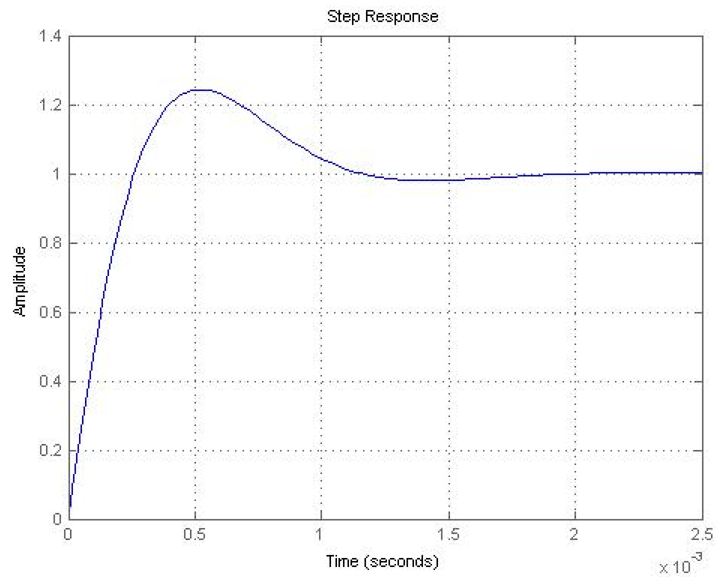

Figure 5.9: The Step response of the Closed loop system

Then, the cutoff frequency ω_g of the simplified transfer function can be obtained by interpolating the Bode plot:

$$-20 \cdot log(\frac{\omega_1}{\omega_g}) = |G_{i,c}(j\omega_1)| \tag{5.45}$$

Therefore, ω_g can be calculated from

$$\omega_g = 10^{[log(\omega_1) - \frac{|G_{i,c}(j\omega_1)|}{20}]} \tag{5.46}$$

Therefore, the simplified transfer function (5.43) can be determined with the cutoff frequency ω_g. Based on (5.26), and the load equation

$$T_e - T_L = J\dot{\omega}_m \tag{5.47}$$

The open loop transfer function for speed control is given as follows

$$G_w(s) = G_{i,sim}(s)\frac{3}{2}\frac{P}{2}\frac{L_m}{L_r}\lambda_d^r\frac{1}{sJ} \tag{5.48}$$

where P is the number of poles

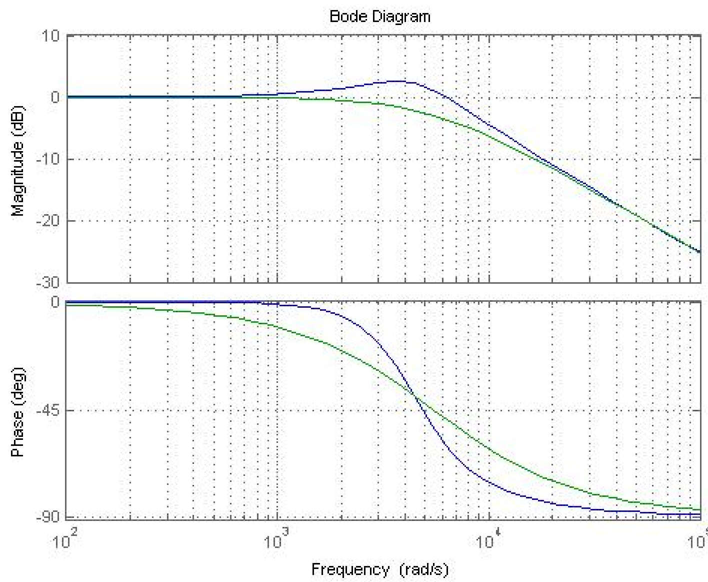

Figure 5.10: The Comparison of Higher order and Simplified system response

Now introducing the PI speed controller into the system, the open loop transfer function of the overall plant is shown below:

$$\begin{aligned} G_{w,o}(s) =& R_w(s)G_w(s) \\ =& K_p^w(1+\frac{1}{sT_i^w})\frac{1}{1+\frac{s}{\omega_g}}\frac{3}{2}\frac{P}{2}\frac{L_m}{L_r}\lambda_d^r\frac{1}{sJ} \\ =& K_p^w\frac{3PL_m\lambda_d^r}{4L_rJ}(1+\frac{1}{sT_i^w})(\frac{1}{1+\frac{s}{\omega_g}}) \\ =& K_p^w\frac{3PL_m\lambda_d^r}{4L_rJ}\frac{1+sT_i^w}{sT_i^w(s+\frac{s^2}{\omega_g})} \end{aligned} \tag{5.49}$$

The symmetrical optimum method is used for determining the parameters for PI speed controller. The method can produce the balance phase and magnitude characteristic of the open loop transfer function, by placing the crossover frequency precisely at the location where we can obtain the maximum phase margin. The slope of -20 dB/decade produced by PI controller becomes -40 dB/decade after the cutoff frequency ω_g of current control loop low-pass filter.

We introduce a factor α that relates the cross-over frequency ω_c and the PI speed controller cutoff frequency ω_w with the first-order system cutoff frequency ω_g, where

$$\omega_c = \frac{1}{\alpha}\omega_g, \omega_w = \frac{1}{\alpha^2}\omega_g$$

On logarithmic scale, ω_c is exactly the middle point between ω_w and ω_g. Applying these two conditions to the open loop transfer function, we have:

$$|(G_{w,o}(j\omega_c)| = |G_{w,o}(\frac{j\omega_g}{\alpha})| = 1 \tag{5.50}$$

$$arg(G_{w,o}(j\omega_c)) = arg(G_{w,o}(\frac{j\omega_g}{\alpha})) = -\frac{2\pi}{3} \tag{5.51}$$

Firstly, α is solved from the phase margin condition, i.e.,

$$\begin{aligned} arg(G_{w,o}(j\omega_c)) =& arg(1 + j\omega_c T_i^w) - arg(1 + j\omega_c T_g) - \pi \\ =& tan^{-1}(\omega_c T_i^w) - tan^{-1}(\omega_c T_g) - \pi = -\frac{2\pi}{3} \end{aligned} \tag{5.52}$$

Since $\omega_c = \frac{\omega_g}{\alpha} = \frac{1}{\alpha T_g}$ and $T_i^w = \alpha^2 T_g$ we get,

$$tan^{-1}(\alpha) - tan^{-1}(\frac{1}{\alpha}) = \frac{\pi}{3} \tag{5.53}$$

Based on trigonometric rules, we can obtain α value. The controller parameter K_p^w can be determined by substituting the α in the magnitude condition (5.50).

$$\begin{aligned} |G_{w,o}(\frac{j\omega_g}{\alpha})| = |G_{w,o}(\frac{1}{j\alpha T_g})| =& K_p^w \frac{3pL_m}{4L_r}\frac{\lambda_d^r}{J}T_g\sqrt{\frac{1+\alpha^2}{1+\frac{1}{\alpha^2}}} = 1 \\ K_p^w =& \frac{1}{\frac{3pL_m}{4L_r}\frac{\lambda_d^r}{J}T_g\sqrt{\frac{1+\alpha^2}{1+\frac{1}{\alpha^2}}}} \end{aligned} \tag{5.54}$$

Therefore, based on the calculated T_i^w and K_p^w values, we can obtain K_i^w from

$$K_i^w = \frac{K_p^w}{T_i^w} \tag{5.55}$$

The Bode plot of closed loop speed control system is shown in the Fig.7, and the step response is shown in Fig.8.

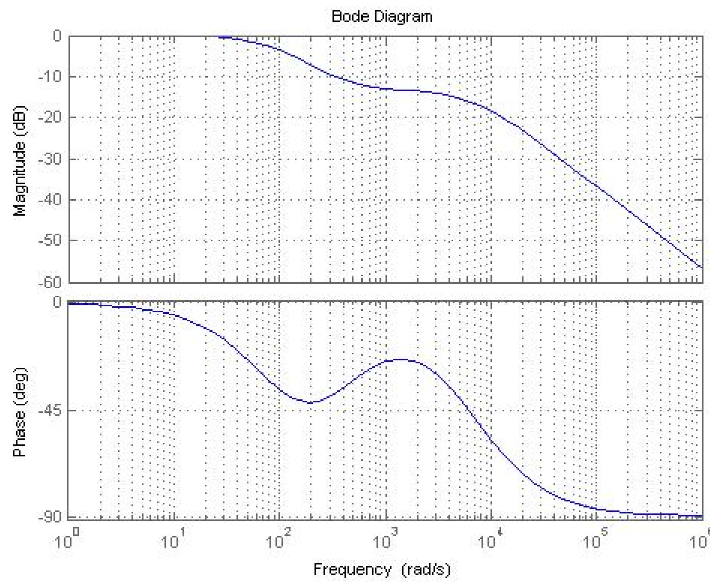

Figure 5.11: The Bode plot of Speed control system

5.3 Simulation Results

The effectiveness of the proposed control scheme of induction motor control are demonstrated by computer simulations. The model parameters are summarized in Appendix B. Based on previous control design methods, the controller parameters are calculated and summarized in Tab 5.1 The computer simulation results are summarized

Table 5.1: The Calculated K_p and K_i Values

	K_p	K_i
current controller(I)	235.98	8.56×10^5
speed controller(ω)	0.4150	176.2084

in Fig. 5.11 and Fig. 5.12. Fig. 5.14 shows the actual speed matches the reference speed very well. Fig. 5.11 shows the actual rotor angle plot. Fig. 5.16 and Fig. 5.17 show the

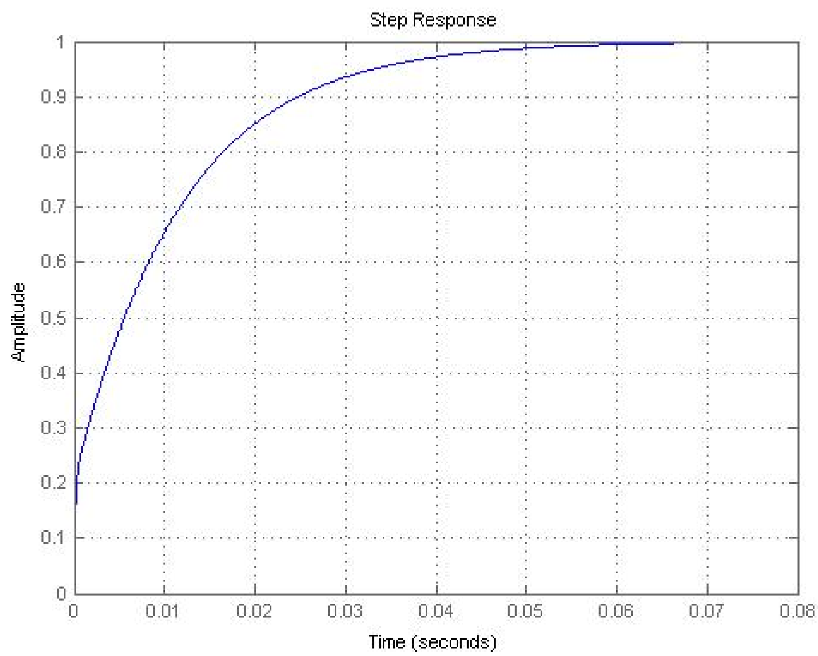

Figure 5.12: The Step response of Speed control system

quadrature and direct axis correspondingly. We can see that the direct axis current in Fig. 5.17 matches the reference $i_d^{s*} = 0$ very well.

5.4 Summary

The concept and model of field oriented control of induction motor are presented. The feed-forward control method is designed for decoupling for torque and flux of induction motor. A novel PID based field oriented control approach of induction motor is proposed in this paper. A PID based controllers have been developed for speed and current control loop based on symmetrical optimum method, which guarantees the maximum phase margin. The simulation results show the robustness and effectiveness of the controllers design.

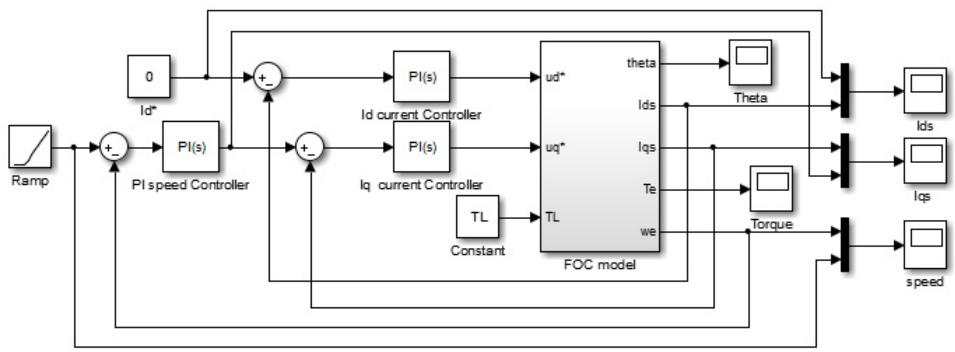

Figure 5.13: Filed Oriented Control of Induction Motor

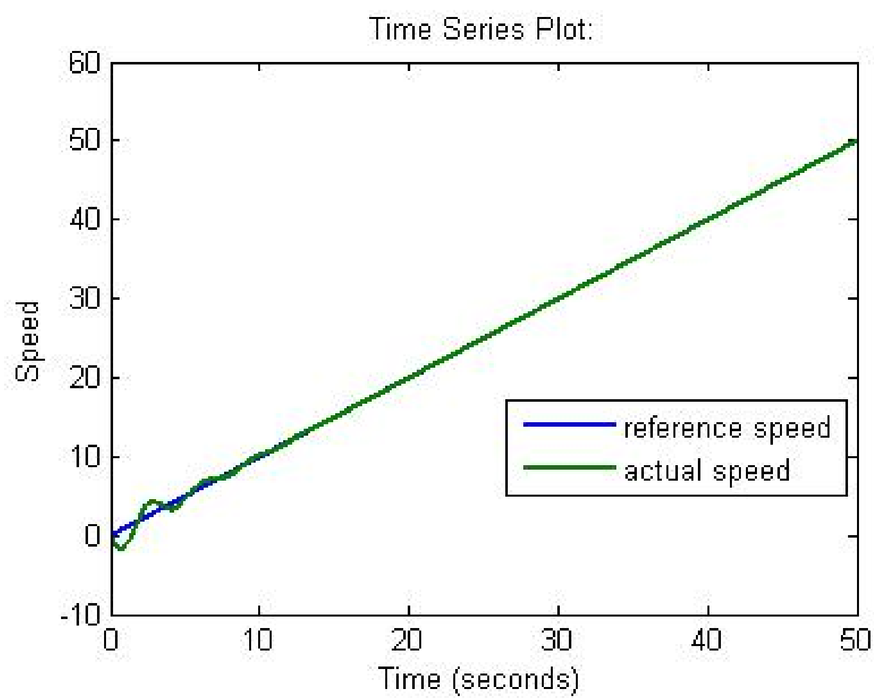

Figure 5.14: Speed of Induction Motor

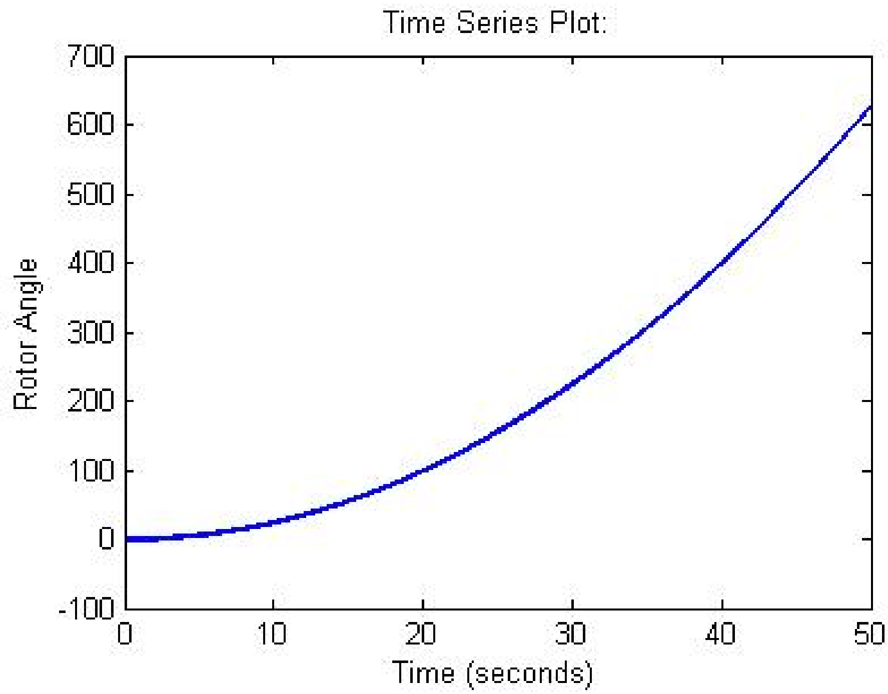

Figure 5.15: Angle of Induction Motor

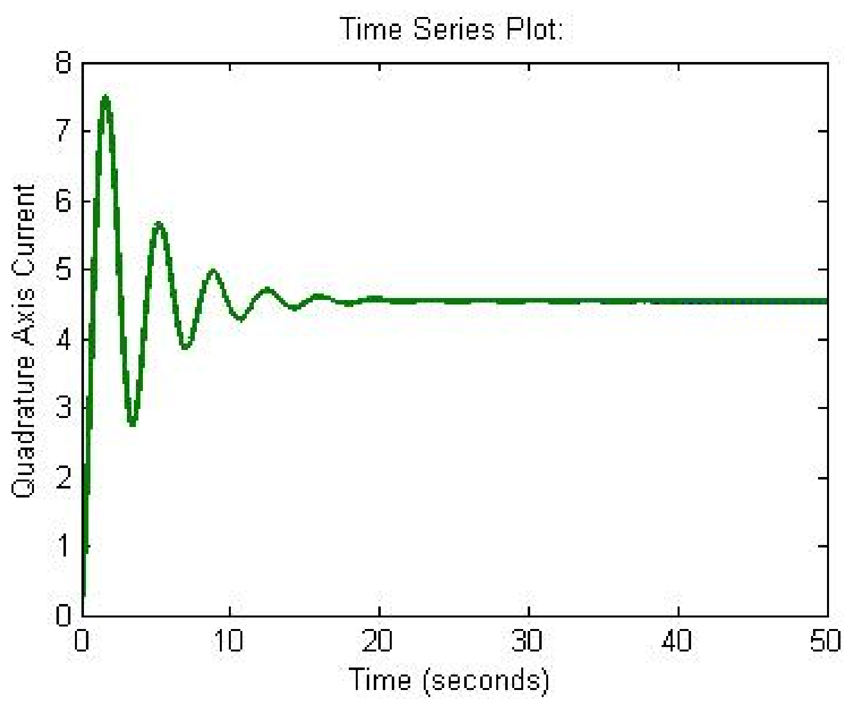

Figure 5.16: Quadrature Axis Current

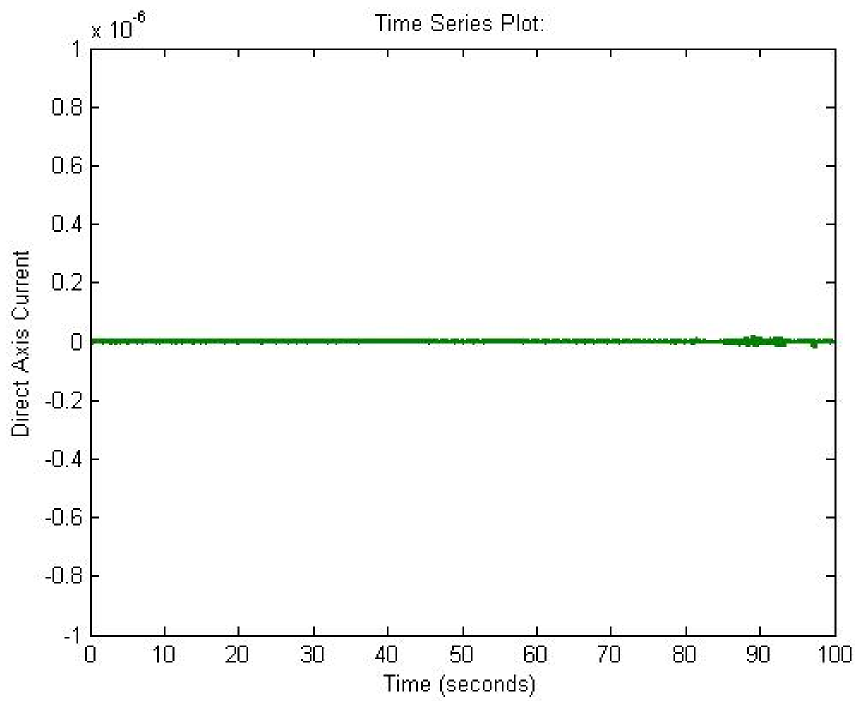

Figure 5.17: Direct Axis Current

CHAPTER 6

IMPLEMENTATION WITH DSP CONTROLLERS

6.1 Introduction

The field-oriented control technique is implemented using the digital motor control (DMC) and power factor correction (PFC) equipment (TMDSHVMTRPFCKIT) made by Texas Instruments. The DMC board uses the 32-Bit C2000 DSP controllers, because DSP controllers can compute complex control algorithms with the mixed peripherals, which can interface with different components of DMC hardware and also meet the safety requirements. The total kit required consists of the following contents.

- F28035 control card or F28335 control card
- High voltage DMC board
- 15V Power Supply

The Texas instruments AC motor development kit assembly provided with required contents is shown in the Fig. 6.1. The figure primarily shows the high voltage digital motor control board (HVDMC), which is shaped inside plastic enclosure. The heat sink is provided below the HVDMC board to the motor inverter with a DC fan attached to increase the airflow in the heat sink. The HVDMC board allows any of the C2000 series control cards. The Texas Instruments (TI) developed a software named Code Composer Studio (CCS) which supports processors portfolio. CCS is an integrated development environment (IDE) which can make use of C/C++ compiler, source code editor, debugger, project build environment, profiler, and plenty other features. Now let's look into the construction of HVDMC board.

Hardware Analysis :

The Fig 6.2 explains the how we are controlling the motor drive system gradually. The

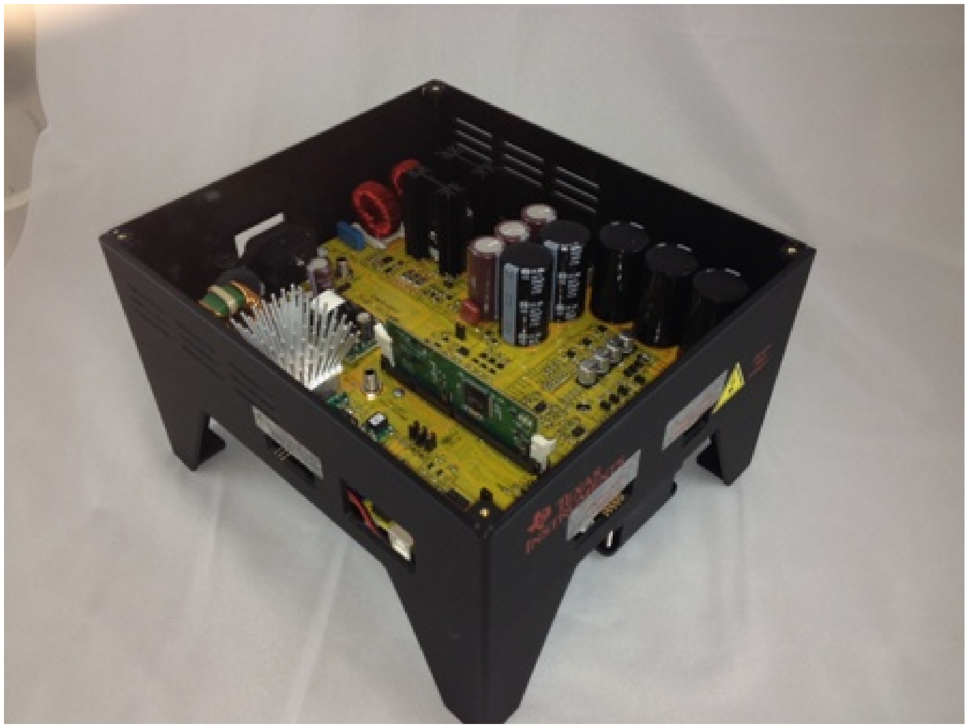

Figure 6.1: The Texas Instruments AC motor Development Kit

power supplied from AC mains is first given to the AC rectified stage and passed power factor correction stage (PFC). The output of the PFC stage is given to the three-phase inverter which is connected the motor. The operation of each stage is explained below

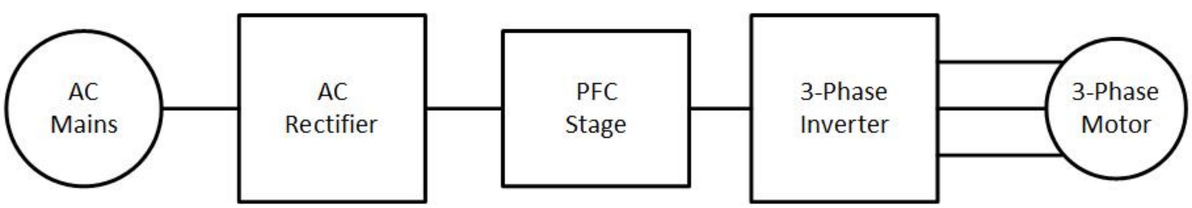

Figure 6.2: Block Diagram of Motor Drive System using PFC

- AC Rectifier stage which rectifies the AC power taken from the mains. This can be used as input to the power factor correction stage or to supply the DC bus voltage required to the inverter directly.

- Power Factor Correction stage increases the efficiency by wave shaping the input

AC current and regulates the DC bus of the inverter for efficient operation.

- 3-Phase Inverter Stage controls the input high voltage given to the motors.
- Auxiliary Power Supply Module generates small DC voltage of 15V or 5V form AC rectifier voltage stage or PFC output

There are few other Miscellaneous like Over current protection, Isolated CAN interface and Four PWM DAC's to complete the motor control drive system. The next section explains how the HVDMC board is built based on the required hardware components for Motor control.

6.1.1 High Voltage Digital Motor Control

The HVDMC kit is categorized into several functional macro blocks, so that one stage can easily debug and tested at a time. That completes the total requirement for controlling motor drive system. The functioning of each macro block is listed below.

Main - This block consists of control CARD connection, jumpers, communications(iso CAN), Instrumentation (DAC'S), QEP and CAP connection and voltage translation

M1 -This block rectifies the AC supply taken from the mains into the DC. The rectified DC is fed as input to the Power Factor Correction stage or to the inverter directly.

M2 - This block has auxiliary power supply, 400V to 5V and 15V module that can produce 15V, 5V for the rectified AC power.

M3 - This block has an isolated USB emulation which provide isolated JTAG connection to the controller or isolated SCI when JTAG is not required.

M4 - This two-phase interleaved PFC stage which is used to increase the efficiency of operation.

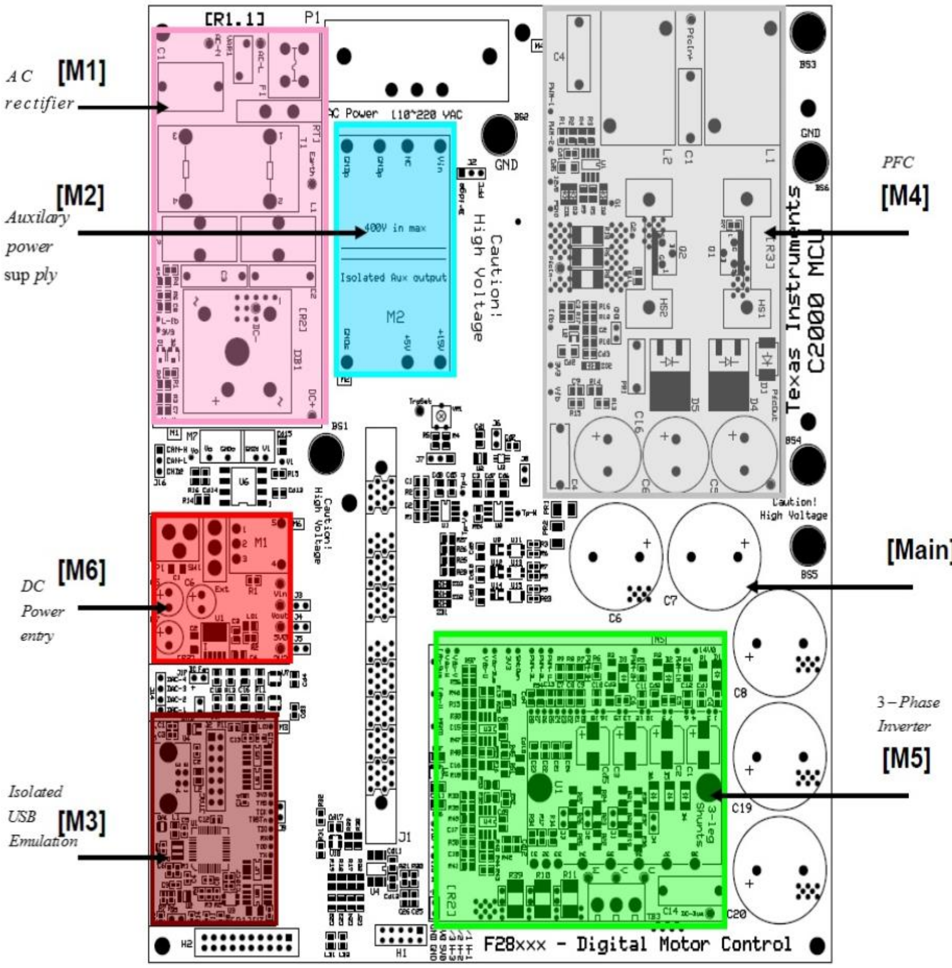

Figure 6.3: The Layout of HVDMC Board

M5 - This block consists of a three-phase inverter which is fed to the input of three phase motor.

M6 - This block generates DC voltage of 15V, 5V and 3.3V for the board. It has DC power entry fed from external DC power supply.

The banana jack connectors are used to connect the power stages for completion of total hardware configuration. The Fig 6.3 represents the layout of the HVDMC board and location of macro blocks on the board.

6.1.2 C2000 DSP Controllers

The HVDMC board uses the C2000 family of DSP controllers, which can solve the complex control algorithms fast and can be easily implemented. They can be used to for scalar or vector control applications and preferably designed for real-time operation. These can provide the following advantages to the system

- The system cost is reduced by efficient control in all speed range
- The high resolution PWM's can be generated for controlling power switching inverters
- Any sensor inputs can be solved with high quality using the dual sample hold, 12-bit, high speed ADC's.
- The memory required is reduced due to decreasing in the number of lookup tables.

Use of advanced control algorithms

- Reduces the torque ripple which lowers the vibrations and increase the lifetime of the motor.
- Reduces harmonics generated by the inverter which decreases the filter cost
- sensorless algorithms exclude the need of speed or position sensor

The TMS320F28035 DSP controller is used, and the functional block diagram is shown in the Fig 6.4. The TMS320F28035 DSP is a family of F2803x DSP micro controller available with power of $C28x^{TM}$. This family provided the high level of analog integration, and Control Law Accelerator (CLA) is coupled with highly integrated peripherals in small count of pins. The some features of controller are given[31].

Name	TMS320F28035
Clock Speed	60 MHz
Memory	on-chip
Analog to digital conversion	16 channels
PWM	14 channels
Input/output pins	Up to 56 pins
Signal level	[0, 3.3] V (0-3.3 V on ADC pin)

6.2 Summary

The Texas instrument motor development kit and software are introduced in this chapter. The key features of DSP controller are summarized. Our design is implemented based on the hardware with CCS program. The hardware experiment shows satisfactory performance in speed control.

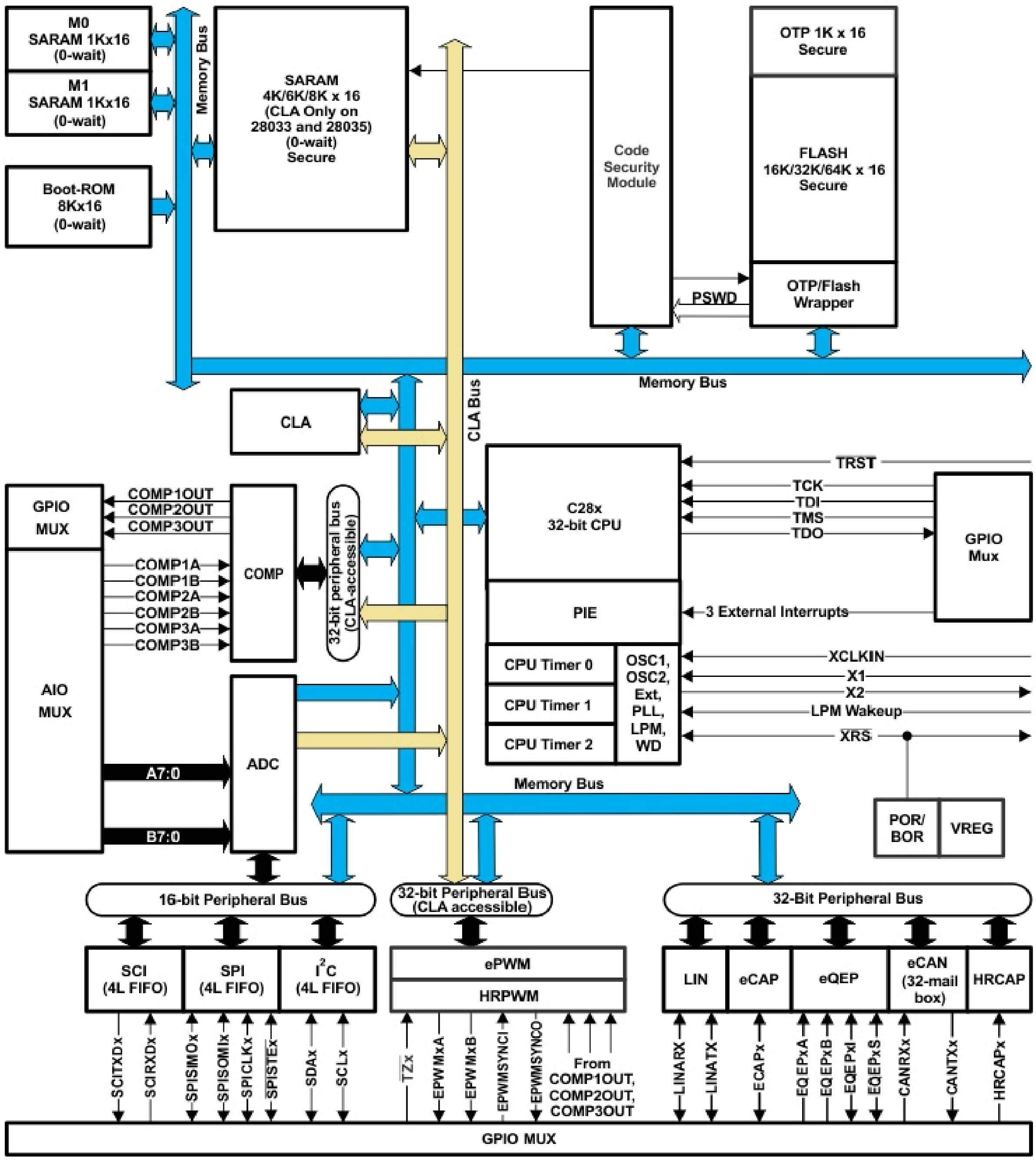

Figure 6.4: Functional Block Diagram of TMS320F28035

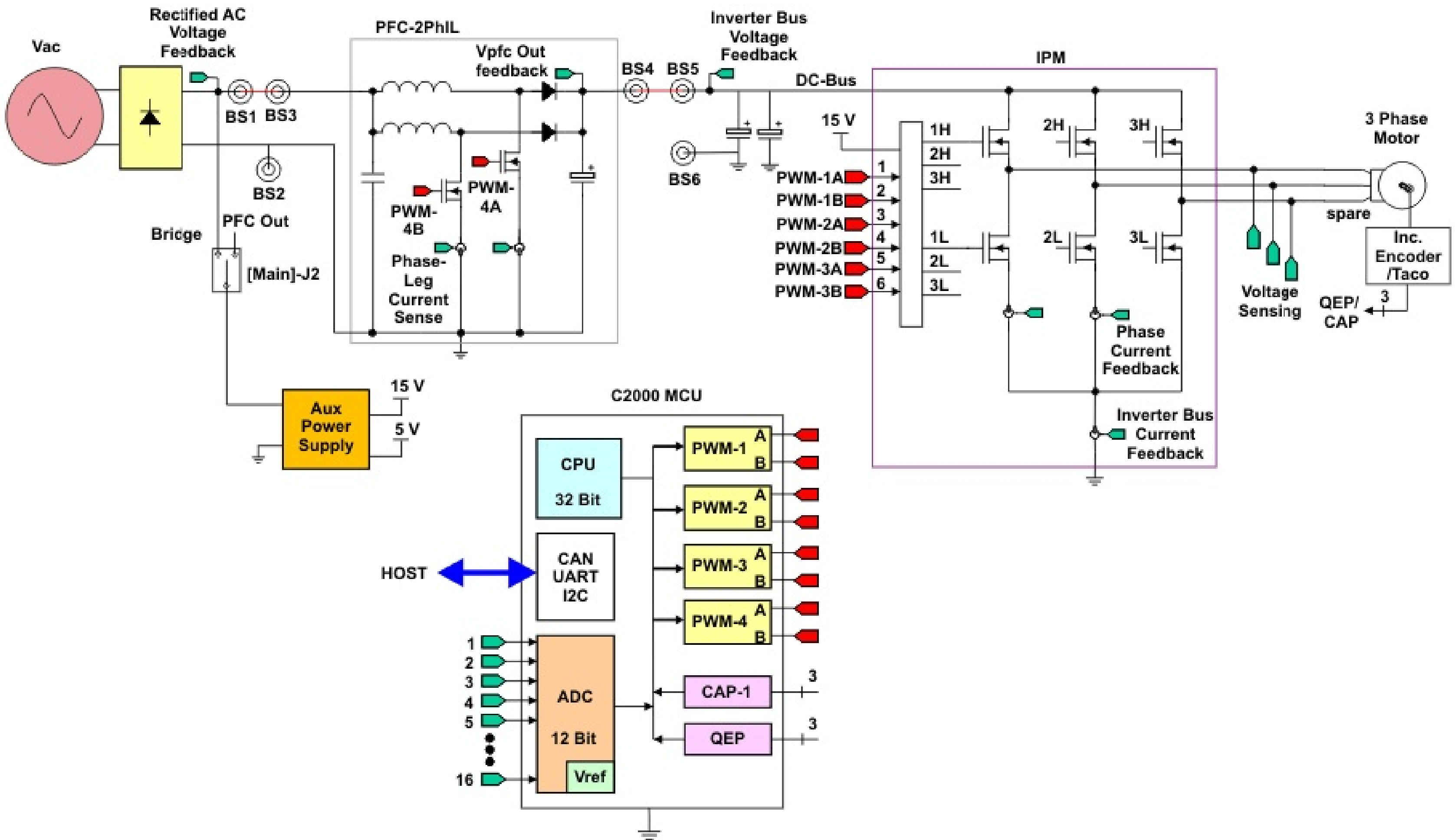

Figure 6.5: HVDMC+PFC Board Block Diagram with C2000 MCU

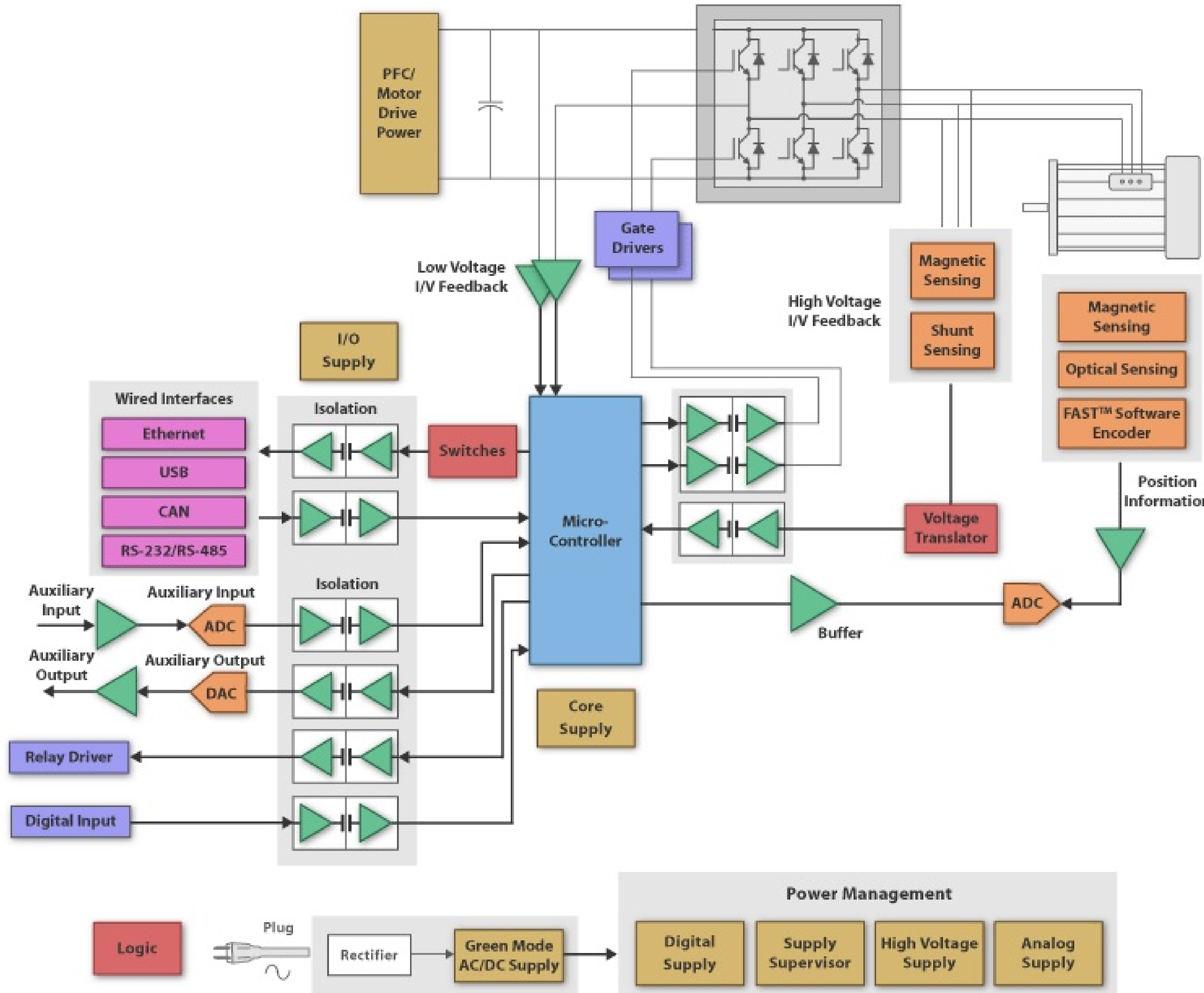

Figure 6.6: The Complete Control Block Diagram of AC Induction Machine

CHAPTER 7

CONCLUSION

A novel field oriented control technique of induction motor is presented in this thesis. The dynamic model of induction motor is developed in synchronous rotating frame, i.e., dq coordinate frame. The Clarke's and Park's transformations are used to convert the abc coordinate frame into the rotating dq frame. The transformation greatly reduces the complexity of the dynamic model.

The characteristics of IGBT are studied in the thesis. The 120^0 and 180^0 conduction of three-phase voltage source inverter theories are summarized in Chapter 4 and results are presented using Matlab/Simulink. The concepts of Space Vector Pulse Width Modulation (SVPWM) are discussed. The Space Vector PWM technique is developed to control the switching of three-phase inverter and is simulated with Matlab/Simulink.

The thoery of field oriented control is introduced and applied to control the dynamic model of induction motor. Both of the direct and indirect field control methods can be applied to calculate the rotor flux angle. The decoupled system can be achieved after applying the feed-forward control method. PID based controllers have been designed for speed and current control based on symmetrical optimum method, which guarantees the maximum phase margin. The developed PI controllers for speed and current control show satisfactory performance. The simulation results shows the robustness and effectiveness of the controllers design.

The Texas Instruments AC motor development kit and software are used to implement the field oriented control of induction motor in hardware platform. The DSP hardware implementation demonstrates that our novel field oriented control of induction motor can control the speed and torque effectively.

REFERENCES

[1] K.H. Nam, *AC Motor Control and Electric Vehicle Application*, CRC Press, 2010.

[2] A M. Trzynadlowski, *Control of Induction Motors*, Academic Press 2001

[3] John Chiasson, *Modeling and High-Performance Control of Electric Machines*, IEEE press 2005.

[4] Robins. B, Francois. B, Degobert. P and Hautier. J.P, *Vector control of Induction machines, Power systems*, 10.1007/978-0-85729-901-7_2, Springer-Verlag London 2012

[5] Rashid M. H, *Power Electronics Handbook*, San Diego: Academic Press, (2001).

[6] Bin Wu, *High-Power Converters and ac Drives*, The Institute of Electrical and Electronics Engineers, INC 2006.

[7] A. Iqbal, A. Lamine, I. Ashraf and Mohibullah, *Matlab/Simulink model of space vector PWM for three phase voltage source inverter*

[8] Park .R, *Two-reaction theory of synchronous machines Generalized method of analysis-Part I*, AIEE Trans, Vol. 48, pp.716-724, July 1929,.

[9] S J. Chapman, *Electric Machinery Fundamentals*, Mc Graw-Hill, NY 10020, 2012.

[10] K Ogata, *Modern Control Engineering*, Pearson, NJ 07458, 2010.

[11] S. Nandi, *Modeling of induction machines including stator and rotor slot effects*, IEEE Transactions on Industry Applications, vol. 40, no. 4, pp. 10581065, July/August 2004.

[12] Texas Instruments, *Field oriented control of induction motor*, Retrieved from (http://www.tij.co.jp/jp/lit/an/bpra073/bpra073.pdf)

[13] Bilal Alkin and Manish Bhardwaj, *Sensored Field oriented control of 3-phase induction motor*, Texas Instruments, SPRABP8-july 2013.

[14] Sattar. A, *Insulated Gate Bipolar Transistor (IGBT) Basics*, IXYS Corporation, IXAN0063. Retrieved from `http://www.ixys.com/Documents/AppNotes/IXYS_IGBT_Basic_I.pdf`

[15] Moorthi V. R, *Power electronics: Devices, circuits and industrial applications*, Delhi, Oxford University Press, (2005).

[16] Wilamowski B. M, and Irwin J. D. *Power Electronics and Motor Drives*, Boca Raton, FL : CRC Press (2011).

[17] Bimbhra P. S, & Kaur S. *Power electronics*, New Dehli: Khanna, (1999).

[18] Jisha. L.K, P.Thomas, *A Comparative Study on Scalar and Vector Control of Induction Motors*

[19] Texas Instruments, *Implementation of speed field oriented control of three phase induction motor using TMS320F240*. Retrieved from (http://www.ti.com/lit/an/bpra076/bpra076.pdf)

[20] S. Preitl,A-I. Stinean,R-E. Precup, Z. Preitl,E. M-Petriu, C-A. Dragos and M-B Radac, *Controller Design Methods for Driving Systems Based on Extensions of Symmetrical Optimum Method with DC and BLDC Motor Applications*, IFAC Conference Brescia, Italy: March, 2012.

[21] S. Preitl and R-E. Precup, *An extension of tuning relation after symmetrical optimum method for PI and PID controllers*, Automatica 35(1999), pp.1731-1736.

[22] Honrio D.A, Diniz E.C Jnior, A.B.S. Almeida, O. M and Barreto L.H.S.C *Comparision between sliding mode control and vector control for DSP-based position control applied to squirrel-cage induction motor*, 978-1-4244-8010-4/10, IEEE 2010.

[23] D. Asija, *Speed Control of Induction Motor using Fuzzy-PI Controller*, ICMEE 2010.

[24] M M. Rostami, *Analysis of Indirect Rotor Filed Oriented Control for Squirrel Cage Induction Motor Drives*, PEOCO2012, Melaka, Malaysia.

[25] K. Jezernik and G. Edelbaher, *Speed Sensorless Torque and Flux Control of Induction Motor*, 0-7803-7912-8/03, IEEE 2003

[26] V-R. Miguel, M. Mijalkovic, A M. Stankovic, S. Hiti, and J. Nagishma *Ouput selection for Tuning of Filed Oriented Controllers:Steady State Analysis*, 0-7803-7883-0/03, IEEE 2003.

[27] J. Dannehl and F W. Fuchs, *Flatness-Based Control of an Induction Machine Fed via Voltage Source Inverter-Concept, Control Design and Performance Analysis*, 1-4244-0136-4/06, IEEE 2006.

[28] M. Masiala, B. Vafakhah, J. Salmon and A. Knight, *Fuzzy Self-Tuning Speed Control of an Indirect Field-Oriented Control Induction Motor Drive*, 0197-2618/07, IEEE 2007.

[29] F. Blashke, *The Principle of Filed Orientation as applied to the new trans vector closed loop control system for rotating field machine*, Siemens Rev, Vol 39,no.5,pp.217-220, May 1992.

[30] N. Noroozi-Varcheshme, A. Ranjbar-Noiey and H. Karimi-Davijani, *Sensorless Indirect Filed-Oriented Control of Induction Motor using Intelligent PI Controller* ,

[31] Texas Instruments, *Piccolo^{TM} Microcontrollers*. Retrieved from (http://www.ti.com/lit/ds/symlink/tms320f28033.pdf)

[32] Texas Instruments, *TMS320C2000 Motor Control Primer*. Retrieved from (http://processors.wiki.ti.com/index.php/TMS320C2000 Motor Control Primer)

[33] Texas Instruments, *AC induction motor (ACIM) overview*, system block diagram. Retrieved from (http://www.ti.com/lsds/ti/apps/motor/ac induction/overview.page)

[34] Texas Instruments, *High voltage motor control kit and PFC developers kit*, kit diagram. Retrived from (http://www.ti.com/tool/tmdshvmtrpfckit)

APPENDIX A

Sample Program for Field Oriented Control

The sample program for field oriented control of induction machine is shown below:

Instance PI regulators to regulate speed, and the d and q axis currents

PI_CONTROLLER pi_spd = PI_CONTROLLER_DEFAULTS;

PI_CONTROLLER pi_id = PI_CONTROLLER_DEFAULTS;

PI_CONTROLLER pi_iq = PI_CONTROLLER_DEFAULTS;

Initializing the PI modules for Id and Iq current regulators and speed regulator.

- Initialize the PI module for Id

  pi_spd.Kp=_IQ(2.0);

  pi_spd.Ki=_IQ(T*speedLoopPrescalar/0.5);

  pi_spd.Umax=_IQ(0.95);

  pi_spd.Umin=_IQ(-0.95);

- Initialize the PI module for Iq

  pi_id.Kp=_IQ(1.0);

  pi_id.Ki=_IQ(T/0.004);

  pi_id.Umax=_IQ(0.3);

  pi_id.Umin=_IQ(-0.3);

- Initialize the PI module for speed pi_iq.Kp=_IQ(1.0);

  pi_iq.Ki=_IQ(T/0.004);

  pi_iq.Umax=_IQ(0.80);

  pi_iq.Umin=_IQ(-0.80);

Connecting inputs of PI module and callling the macro functions for speed, Iq current and Id current.

- For speed PID IQ controller macro

  if(speedLoopCount=SpeedLoopPrescaler) pi_speed.Ref=rc1.SetpointValue;

  pi_spd.Fbk=speed1.speed;

  PI_MACRO(pi_spd)

  SpeedLoopCount=1;

  else SpeedLoopCount++;

- For PID IQ controller macro function

  pi_iq.Ref=pi_spd.out;

  pi_iqFbk=park1.Qs;

  PI_MACRO(pi_iq)

- For PID ID controller macro function

```
pi_id.Ref=IdRef;

pi_idFbk=park1.Ds;

PI_MACRO(pi_id)
```

APPENDIX B

The Parameters of Induction Motor

Table B.1: The Parameters of the Induction Motor for DSP Control Implementation

variable	value
R_s	11.05 Ω
R_r	6.11 Ω
L_s=L_r	0.3164H
L_m	0.2939H
p	4
f_s	10kHz
J	0.91 Kg.m^2